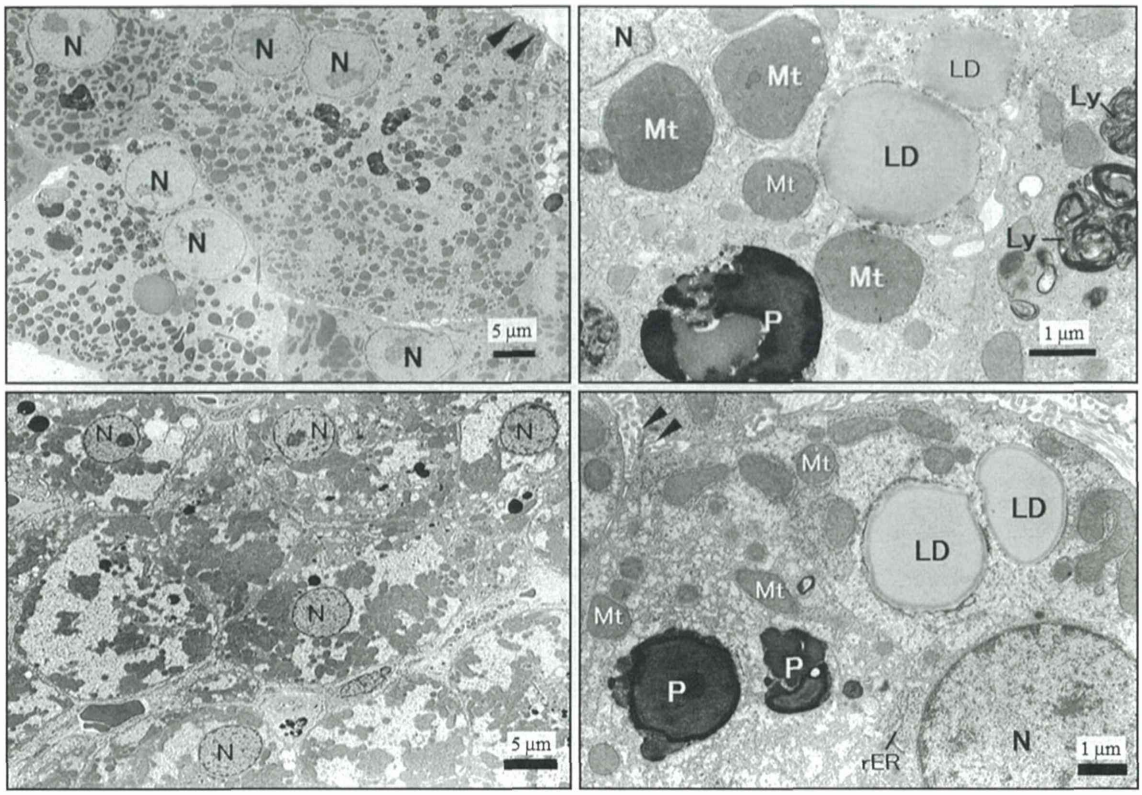

Fig. 3 Ultrastructure comparison between primary hepatic cells (*upper*) and hepatocytes in liver tissue (*lower*) of small Indian mongoose. *N* nucleus, *Mt* mitochondria, *Ly* lysosome, *LD* Lipid droplet, *P* waste pigment, *rER* rough-surfaced endoplasmic reticulum. Microvilli are indicated with *arrow heads*

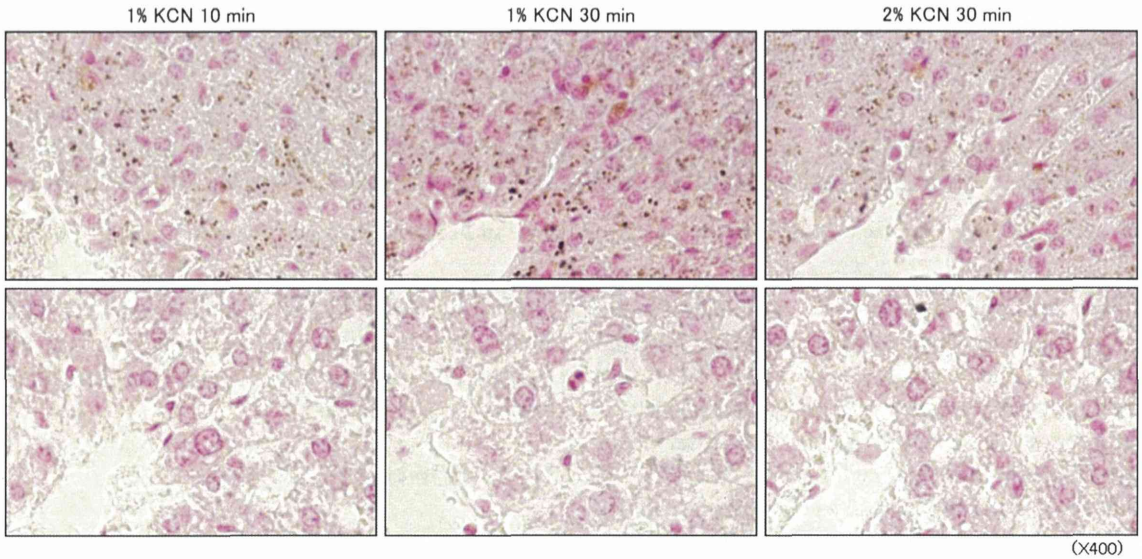

Fig. 4 Comparison between AMG staining of the liver in the small Indian mongoose (*upper*) and rat (*lower*). *Upper* Liver of a female mongoose; Hg concentration was 4.34 μg g^{-1} DW. *Lower* Liver of a female rat; Hg concentration was 0.07 μg g^{-1} DW

dissolved in KCN and so the particles found in mongoose liver were expected to be BiSe, HgS or HgSe. Hg concentration in the mongoose liver was 4.34 μg g^{-1} DW and in the rat was 0.07 μg g^{-1} DW. In our previous study, Bi levels in the 11 liver samples of 18 mongooses were below the detection limit (<0.001 μg g^{-1}) of ICP-MS (ICP-MS;

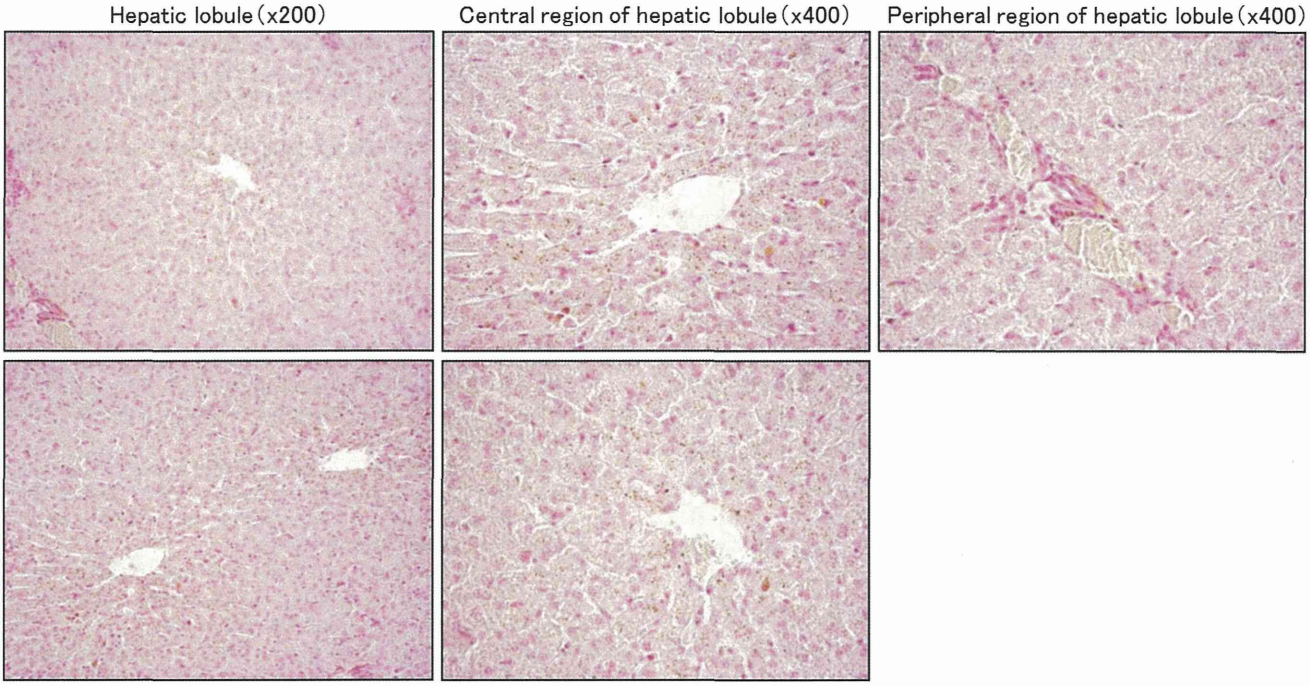

Fig. 5 Distribution of Hg in the liver of the small Indian mongoose detected with AMG staining

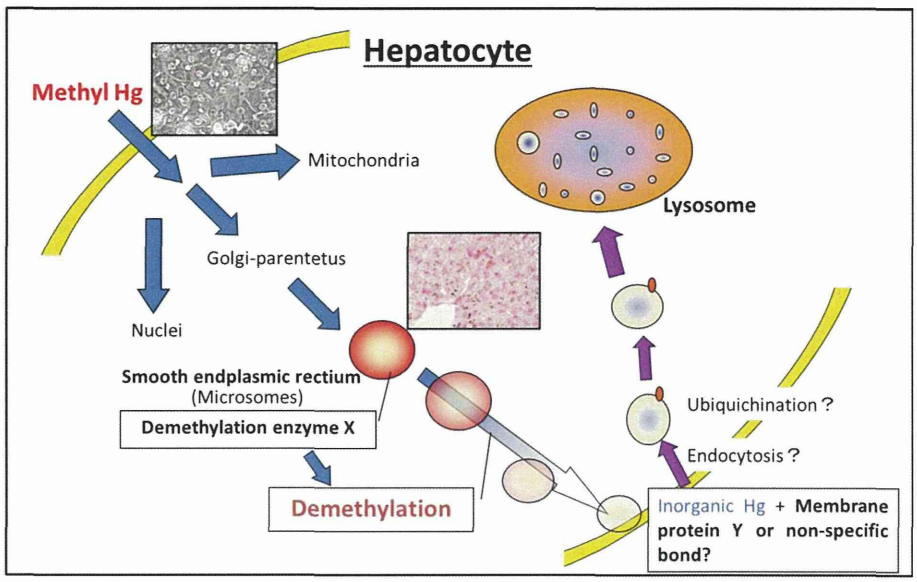

Fig. 6 A hypothesis for methylmercury metabolism in the hepatocytes of the small Indian mongoose

Agilent 7500cx, Agilent Technologies), and mean Bi level in the remaining samples ($n = 7$) was 0.01 μg g^{-1} DW (Unpublished data). This mean value was lower than the Hg concentration, 0.07 μg g^{-1} DW, in rat liver and there was no observation of any metal particles. These results suggest, therefore, that the KCN and HCl resistant particles are compounds of Hg not Bi.

Many particles were accumulated in the central region of hepatic lobules (Fig. 5). Smooth endoplasmic reticulum, which plays a role in xenobiotic metabolism, lipid/cholesterol metabolism, and the decomposition and detoxification of lipophilic substances, grows in the central region of hepatic lobules (Wakui and Kaneda 2001). It suggests that the distribution of Hg compounds in hepatic lobulesis similar to that of smooth endoplasmic reticulum. With regard to Hg compounds with Se and S in terrestrial mammals, it has been reported that most of the Hg in the soluble fractions of rat organs is found as Hg–Se compounds bound to proteins (Naganuma and Imura 1981), and Hg–Se–S compounds were identified in the plasma of

rabbits (Gailer et al. 2000). On the contrary, insoluble Hg–Se, (–S) granules have been found in the livers of marine animals which have higher Hg content in their livers such as in striped dolphin (Ng et al. 2001), northern fur seal and black-footed albatross (Arai et al. 2004). In the present study, insoluble Hg compounds with Se or S were found in the liver of mongoose which is a terrestrial mammal. This result suggests that the Hg metabolism and detoxification system of mongoose is similar to those of marine animals.

We reported that the O-Hg/T-Hg ratio in liver microsomes was the lowest of five organelle fractions (nucleus, cytosol, mitochondria, plasma membrane, and microsome) (Horai et al. 2008). When viewed under a transmission electron microscope, the proximal tubular cells of patients who suffered from inorganic Hg intoxication had Hg-positive lysosomes that were characterized by a dense matrix (Aoi et al. 1985). On the basis of these collective results, we derived previously a hypothesis for Hg metabolism in a cell (Fig. 6) (Horai et al. 2008). Methyl Hg easily permeates into cells through lipid bilayer because of its high liposolubility (Komatsu et al. 1975). Methyl Hg is distributed in organelle, mainly cytosol and microsome (Horai et al. 2008). Methyl Hg may be demethylated in microsomes (smooth endoplasmic reticulum), which moves in cytosol and then is taken into plasma membrane. Therefore, the chemical form of Hg in plasma membrane is dominantly inorganic (Horai et al. 2008). Finally, demethylated inorganic Hg may assemble in lysosomes via endocytosis. Several views on the distribution and mineralization of Hg–Se (–S) in lysosome of marine animals has already been reported (Ikemoto et al. 2004a). These findings in the present study may be a breakthrough in the understanding of Hg metabolism and detoxification mechanisms in wildlife which have high Hg contents in their livers.

Conclusions

We successfully established a primary cell culture of mongoose hepatocytes. It was revealed that Hg compounds such as HgSe and/or HgS in mongoose liver tissue mainly distributed in the central region of hepatic lobules than at the periphery. This suggests that the Hg compounds coexist with smooth endoplasmic reticulum in hepatic lobules. Moreover, there is a possibility that smooth endoplasmic reticulum has a role in demethylation of methyl Hg.

Acknowledgments This work was supported by the Global Environment Research Fund (RF-085 and RF-0908) of the Ministry of the Environment, Japan. This work was also supported by a Grant-in-Aid for Scientific Research for Young Scientists (B) 23710044 provided by the Ministry of Education, Culture Sports, Science, and Technology (MEXT), Japan. This study was also partially supported by the Global Center of Excellence (COE) Program of the Japanese Ministry of Education, Culture, Sports, Science and Technology (MEXT), Japan to Ehime University, Japan. The authors wish to thank Dr. A. Subramanian, Ehime University, Japan for critical reading of the manuscript.

Conflict of interest The authors declare that they have no conflict of interest.

References

Aoi T, Higuchi T, Kidokoro R, Fukumura R, Yagi A, Ohguchi S, Sasa A, Hayashi H, Sakamoto N, Hanaichi T (1985) An association of mercury with selenium in inorganic mercury intoxication. Hum Toxicol 4:637–642

Arai T, Ikemoto T, Hokura A, Terada Y, Kunito T, Tanabe S, Nakai I (2004) Chemical forms of mercury and cadmium accumulated in marine mammals and seabirds as determined by XAFS analysis. Environ Sci Technol 38:6468–6474

Blévin P, Carravieri A, Jaeger A, Chastel O, Bustamante P, Cherel Y (2013) Wide range of mercury contamination in chicks of southern ocean seabirds. PLoS One 8(1):1–11

Cardellicchio N, Dectaldo A, Di Leo A, Misino A (2002) Accumulation and tissue distribution of mercury and selenium in striped dolphins (*Stenella coeruleoalba*) from the Mediterranean Sea (southern Italy). Environ Pollut 116:265–271

Cardellichio N, Giandomenico S, Ragone P, Di Leo A (2000) Tissue distribution of metals in striped dolphines (*Stenella coeruleoalba*) from the Apulian coasts, Southern Italy. Mar Environ Res 49:55–66

Caurant F, Navarro M, Amiard JC (1996) Mercury in pilot whale: possible limits to the detoxification process. Sci Total Environ 186:95–104

Chang TT, Hughes-Fulford M (2014) Molecular mechanisms underlying the enhanced functions of three-dimentional hepatocyte agregates. Biomaterials 35:2162–2171

Chen MH, Shih CC, Chou CL (2002) Mercury, organic-mercury and selenium in small cetaceans in Taiwanese waters. Mar Pollut Bull 45:237–245

Danscher G, Stoltenberg M (2006) Autometallography (AMG) Silver enhancement of quantam dots resulting from (1) metabolism of toxic metals in animals and humans, (2) in vivo, in vitro and immersion created zinc–sulphur/zinc–selenium nanocrystals, (3) metal ions liberated from metal implants and particles. Prog Histochem Cytochem 41:57–139

Das K, Siebert U, Gillet A, Dupont A, Dipoï C, Fonfara S, Mazzucchelli G, Pauw ED, Paue-Gillet MCD (2008) Mercury immune toxicity in hourbor seals: links to in vitro toxicity. Environ. Health 7:52

Decataldo A, Di Leo A, Giandomenico S, Cardellicchio N (2004) Association of metals (mercury, cadmium and zinc) with metallothionein-like proteins in storage organs of stranded dolphins from the Mediterranean sea (Southern Italy). J Environ Monit 6:361–367

Dufresne MM, Frouin H, Pillet S, Lesage V, Guise SD, Fournier M (2010) Comparative sensitivity of harbour and grey seals to several environmental contaminants using in vitro exposure. Mar Pollut Bull 60:344–349

Endo T, Haraguchi K, Sakata M (2002) Mercury and selenium concentrations in the internal organs of toothed whales and dolphins marketed for human consumptions in Japan. Sci Total Environ 300:15–22

Environmenal Protection Agency (US) (1997) Mercury study report to Congress. Environmental Protection Agency (US) Summary Vol 1, Washington

Fant ML, Nyman M, Helle E, Rudbäck E (2001) Mercury, cadmium, lead and selenium in ringed seals (*Phoca hispida)* from the Baltic Sea and from Svalbard. Environ Pollut 111:493–501

Frouin H, Loseto LL, Stern GA, Haulena M, Ross PS (2012) Mercury toxicity in beluga whale lymphocytes: limited effects of selenium protection. Aquat Toxicol 109:185–193

Gailer J, George GN, Pickering IJ, Madden S, Prince RC, Yu EY, Denton MB, Younis HS, Aposhian HV (2000) Structural basis of the antagonism between inorganic mercury and selenium in mammals. Chem Res Toxicol 13(11):1135–1142

Hasgekar N, Beck JP, Dunkelberg H, Hirsch-Ernst KI, Gebel TW (2006) Influence of antimonite, selenite, and mercury on the toxicity of arsenite in primary rat hepatocytes. Biol Trace Elem Res 111:167–183

Horai S, Minagawa M, Ozaki H, Watanabe I, Takeda Y, Yamada K, Ando T, Akiba S, Abe S, Kuno K (2006) Accumulation of Hg and other heavy metals in the Javan mongoose (*Herpestes javanicus*) captured on Amamioshima Island, Japan. Chemosphere 65:657–665

Horai S, Furukawa T, Ando T, Akiba S, Takeda Y, Yamada K, Kuno K, Abe S, Watanabe I (2008) Subcellular distribution and potential detoxification mechanisms of mercury in the liver of the Javan mongoose (*Herpestes javanicus*) in Amamioshima Island. Jpn Environ Toxicol Chem 27(6):1354–1360

Ikemoto T, Kunito T, Tanaka H, Baba N, Miyazaki N, Tanabe S (2004a) Detoxification mechanism of heavy metals in marine mammals and seabirds: interaction of selenium with mercury, silver, copper, zinc, and cadmium in liver. Arch Environ Contam Toxicol 47:402–413

Ikemoto T, Kunito T, Watanabe I, Yasunaga G, Baba N, Miyazaki N, Petrov EA, Tanabe S (2004b) Comparison of trace element accumulation in Baikal seals (*Pusa sibirica*), Caspian seal (*Pusa caspica*) and northern fur seals (*Callorhinus ursinus*). Environ Pollut 127:83–97

Ishibashi O, Nishijima T, Sumida K, Yamashita K, Sudo K, Ogura G, Sunagawa K, Nakada T (2009) Chemical immobilization of the small asian mongoose using anesthetic medicine. Jpn J Zoo Wildl Med 14(2):115–118 (in Japanese)

Karagas MR, Choi AL, Oken E, Horvat M, Schoeny R, Kamai E, Cowell W, Grandjean P, Korrick S (2012) Evidence on the human health effects of low-level methylmercury exposure. Environ. Health Persp 120(6):799–806

Koeman JH, Peeters WHM, Koudstaal-Hol CHM, Tjioe PS, de Goeij JJM (1973) Mercury–selenium correlations in marine mammals. Nature 254:385–386

Komatsu Y, Nakao M, Uezato T, Nakao T (1975) The action of methylmercury on the cell membranes. I. Permeability of methylmercury across the cell membranes in direct comparison with mercury chloride. Ind Health 13:211–219

Krabbenhoft DP, Sunderland EM (2013) Global change and mercury. Science 341:1457–1458

Lemes M, Wang F, Stern GA, Ostertag SK, Chan HM (2011) Methylmercury and selenium speciation in different tissues of beluga whales (*Delphinapterusl eucas*) from the Western Canadian Arctic. Environ Toxicol Chem 30:2732–2738

Lindberg S, Bullock R, Ebinghaus R, Engstrom D, Feng X, Fitzgerald W, Pirrone N, Prestbo E, Signeur C (2007) A synthesis of progress and uncertainties in attributing the sources of mercury in deposition. Ambio 36:19–32

Mason R, Choi AL, Fitzgerald WF, Hammerschmidt CR, Lamborg CH, Soerensen AL, Sunderland EM (2012) Mercury biogeochemical cycling in the ocean and policy implications. Environ Res 119:101–117

Meador JP, Ernest D, Hohn AA, Tibury K, Gorzelany J, Worthy G, Stein JE (1999) Comparison of elements in bottlenose dolphins stranded on the beaches of Texas and Florida in the gulf of Mexico over a one-year period. Arch Environ Contam Toxicol 36:87–98

Miyazaki M, Namba M (1992) Cell culture and its application primary culture of human hepatocytes and its application. Jpn J Cancer Chemother 19(9):1411–1419

Monteiro-Neto C, Itavo RV, de Souza Moraes LE (2003) Concentrations of heavy metals in *Sotalia fluviatilis* (Cetacea: Delphinidae) off the coast of Ceará, northeast Brazil. Environ Pollut 123:319–324

Naganuma A, Imura N (1981) Properties of mercury and selenium in a high-molecular weight substance in rabbit tissues formed by simultaneous administration. Pharmacol Biochem Behav 15(3):449–454

Ng PS, Li H, Matsumoto K, Yamazaki S, Kogure T, Tagai T, Nagasawa H (2001) Striped dolphin detoxificates mercury as insoluble Hg(S, Se) in the liver. Proc. Japan Acad 77 Ser. B: 178-183

Rigét F, Braune B, Bignert A, Wilson S, Aars J, Born E, Dam M, Dietz R, Evans M, Evans T, Gamberg M, Gantner N, Green N, Gunnlaugsdóttir H, Kannan K, Letcher R, Muir D, Roach P, Sonne C, Stern G, Wiig Ø (2011) Temporal trends of Hg in Arctic biota, an update. Sci Total Environ 409:3520–3526

Sashi N, Aleo MD, Strock CJ, Stedman DB, Wang H, Will Y (2013) Toxicity assessments of nonsteroidal anti-inflammatory drugs in isoated mitochondoria, rat hepatocytes, and zebrafish show good concordance across chemical classes. Toxicol Appl Pharm 272:272–280

Sato J, Miyazaki M (1984) Primary culture—liver tissue. In Uchida T, Oishi M, Furusawa M, (eds) Dobutsusaiboriyojitsuyokamanyual, Rialaizu-sya, Tokyo, pp134-150, 454

Seigneur C, Vijayaraghavan K, Lohman K, Karamchandani P, Scott C (2004) Global source attribution for mercury deposition in the United States. Environ Sci Technol 38:555–569

Sonne C, Letcher R, Leifsson PS, Rigét F, Bechshøft TØ, Bossi R, Asmund G, Dietz R (2012) Temporal monitoring of liver and kidney lesions in contaminated East Green land polar bears (*Ursus maritimus*) during 1999–2010. Environ Int 48:143–149

Stoltenberg M, Danscher G (2000) Histochemical differentiation of autometallographically traceable metals (Au, Ag, Hg, Bi, Zn): protocols for chemical removal of separate autometallographic metal clusters in Epon sections. Histochem J 32:645–652

Toyama T, Shinkai Y, Yasutake A, Uchida K, Yamamoto M, Kumagai Y (2011) Isothiocyanates reduce mercury accumulation via an Nrf2-dependent mechanism during exposure of mice to methylmercury. Environ Health Pers 119:1117–1122

Wagemann R, Trebacz E, Lockhart WL (1998) Methylmercury and total mercury in tissues of arctic marine mammals. Sci Total Environ 218:19–31

Wakui M, Kaneda K (2001) Structure, function and materials of the human body. IV liver, gallbladder, pancreas. Nihonijisinposha, Tokyo, p 69

Watari Y, Nagata J, Funakoshi K (2011) New detection of a 30-year-old population of introduced mongoose *Herpestes auropunctatus* on Kyushu Island, Japan. Biol Invasions 13:269–276

Wislocki GB (1950) Saliva-insoluble glycoproteins, stained by the periodic acid Schiff procedure, in the placentas of pig, cat, mouse, rat, and man. J Natl Cancer Inst 10:1341

Woshner VM, O'Hara TM, Bratton GR, Suydam RS, Beasley VR (2001) Concentrations and interactions of selected essential and non-essential elements in bowhead and beluga whales of Arctic Alaska. J Wildl Dis 37(4):693–710

Journal of Human Genetics (2014) 59, 117–118

www.nature.com/jhg

COMMENTARY

A commentary on the promise of whole-exome sequencing in medical genetics

Tadashi Kaname, Kumiko Yanagi and Kenji Naritomi

Journal of Human Genetics (2014) **59**, 117–118; doi:10.1038/jhg.2014.7; published online 6 February 2014

The dawn of next-generation sequencers (NGSs) and innovative sequencing technologies have brought a paradigm shift in medical research and clinical practice. Furthermore, the cost reduction of NGSs enables personalized medicine to come to fruition.

However, whole-genome sequencing (WGS) remains expensive when applied to personal genome analysis. WGS generates a large amount of data that requires high-performance computer processing. Targeted whole-exon capture and sequencing [whole-exome sequencing (WES)] is more cost-effective when compared with WGS because exons represent only ~1–2% of the genome and also higher sequence coverage can be achieved by NGSs. In addition, most Mendelian disorders are caused by exonic mutations or splice-junction mutations, and protein-coding genes harbor ~85% of the mutations that have large effects on disease-related traits.[1] Thus, WES will provide many advantages and lower costs than WGS when analyzing personal genomes.

WES was first successfully used in 2010 to discover the gene responsible for Miller syndrome, a Mendelian disorder.[2] Since then, WES has been increasingly used as a fast and accurate genomic discovery approach to investigate both rare genetic disorders and common diseases.

WES is widely applied across different areas of medicine, because it has the added advantage of reduced cost and requires analysis of a much smaller but essential dataset when compared with WGS. In addition, recent clinical molecular diagnostics have used WES to detect heterogeneous Mendelian diseases.[3,4]

A recent review of WES approaches in medical genetics describes the usefulness of WES in medicine and medical research and the impact of WES on clinical diagnoses.[5] WES approaches have greatly facilitated the discovery of candidate genes or gene variants in Mendelian disorders and rare variants in common diseases and genomic characterization in cancer. Currently, WES is increasingly being applied to disease gene discovery, cancer typing and molecular diagnosis.[5]

Presently, WES is an essential tool in medical genetics, especially in the research of Mendelian disorders. WES or multigene tests using NGSs are widely applied to heterogeneous disorders including deafness or ciliopathy.[5,6] WES is also being increasingly applied to genetic testing for undiagnosed patients.[4,5] Yang *et al.*[4] performed WES in undiagnosed patients whose phenotypes were suggestive of potential genetic disorders and achieved a molecular diagnosis for 62 of 250 (25%) patients.

Because WES detects individual genetic variation, it can be used to construct a variation database of anthropic and ethnic populations. At the same time, because WES can detect groups of genetic variations that are unrelated to the indication for the first diagnostic purpose but are of medical value for individual patient care, such 'incidental findings' pose potential ethical problems that should be strongly considered and discussed in clinical practice.[5,7]

WES is a widely applied technique in medical genetics that is capable of detecting variations in whole exons. However, in practical use, understanding WES methodology and limitations are important. Current WES techniques are not capable of detecting all of the variations surrounding exons. Detecting variation by WES is limited by the experimental methods, probe coverage and/or platforms used.[8–10] Hence, WES may not always detect pathogenic or causative variations in a genetic disease. In addition, because WES is a method to detect genomic sequence variations, when a candidate of causative variation in the disease is detected, it requires verification or support by secondary analyses. In particular, further functional analyses are important to confirm whether the variant is pathogenic or benign.

Nevertheless, WES enables the unprecedented low cost and highly efficient analysis of whole exons. WES can be easily used to comprehensively detect individual variations in exons. It is without doubt that WES is a powerful tool in genome analysis, and it greatly progresses medical genetics.

Although WESs' limitations need to be overcome, we anticipate that WES will be used not only in medical research but also in clinical practice for example, molecular diagnosis (whole-gene test) and personal genomics before WGS becomes a common place in medical genetics. Thus, a paradigm shift in medicine by advancement in both WES and WGS is expected to continue.

T Kaname, K Yanagi and K Naritomi are at Department of Medical Genetics, University of the Ryukyus Graduate School of Medicine, Okinawa, Japan
E-mail: tkaname@med.u-ryukyu.ac.jp

1 Majewski, J., Schwartzentruber, J., Lalonde, E., Montpetit, A. & Jabado, N. What can exome sequencing do for you? *J. Med. Genet.* **48**, 580–589 (2011).
2 Ng, S. B., Buckingham, K. J., Lee, C., Bigham, A. W., Tabor, H. K., Dent, K. M. *et al.* Exome sequencing identifies the cause of a mendelian disorder. *Nat. Genet.* **42**, 30–35 (2010).
3 Kaname, T., Yanagi, K. & Naritomi, K. A commentary on the diagnostic utility of exome sequencing in Joubert syndrome and related disorders. *J. Hum. Genet.* **58**, 57 (2013).
4 Yang, Y., Muzny, D. M., Reid, J. G., Bainbridge, M. N., Willis, A., Ward, P. A. *et al.* Clinical whole-exome

sequencing for the diagnosis of Mendelian disorders. *N. Engl. J. Med.* **369,** 1502–1511 (2013).
5 Rabbani, B., Tekin, M. & Mahdieh, N. The promise of whole-exome sequencing in medical genetics. *J. Hum. Genet.* **59,** 5–15 (2014).
6 Tsurusaki, Y., Kobayashi, Y., Hisano, M., Ito, S., Doi, H., Nakashima, M. *et al.* The diagnostic utility of exome sequencing in Joubert syndrome and related disorders. *J. Hum. Genet.* **58,** 113–115 (2013).
7 Green, R. C., Berg, J. S., Grody, W. W., Kalia, S. S., Korf, B. R., Martin, C. L. *et al.* ACMG recommendations for reporting of incidental findings in clinical exome and genome sequencing. *Genet. Med.* **15,** 565–574 (2013).
8 Teer, J. K., Bonnycastle, L. L., Chines, P. S., Hansen, N. F., Aoyama, N., Swift, A. J. *et al.* Systematic comparison of three genomic enrichment methods for massively parallel DNA sequencing. *Genome Res.* **20,** 1420–1431 (2010).
9 Clark, M. J., Chen, R., Lam, H. Y., Karczewski, K. J., Chen, R., Euskirchen, G. *et al.* Performance comparison of exome DNA sequencing technologies. *Nat. Genet.* **29,** 908–914 (2011).
10 Wooderchak-Donahue, W. L., O'Fallon, B., Furtado, L. V., Durtschi, J. D., Plant, P., Ridge, P. G. *et al.* A direct comparison of next generation sequencing enrichment methods using an aortopathy gene panel- clinical diagnostics perspective. *BMC Med. Genomics* **5,** 50 (2012).

Cell

Premature Termination of Reprogramming In Vivo Leads to Cancer Development through Altered Epigenetic Regulation

Kotaro Ohnishi,[1,2,8] Katsunori Semi,[1,3,8] Takuya Yamamoto,[1,3] Masahito Shimizu,[2] Akito Tanaka,[1] Kanae Mitsunaga,[1] Keisuke Okita,[1] Kenji Osafune,[1] Yuko Arioka,[1] Toshiyuki Maeda,[4] Hidenobu Soejima,[4] Hisataka Moriwaki,[2] Shinya Yamanaka,[1,3,5] Knut Woltjen,[1,6] and Yasuhiro Yamada[1,3,7,*]

[1]Center for iPS Cell Research and Application (CiRA), Kyoto University, Kyoto 606-8507, Japan
[2]Department of Medicine, Gifu University Graduate School of Medicine, Gifu 501-1194, Japan
[3]Institute for Integrated Cell-Material Sciences (WPI-iCeMS), Kyoto University, Kyoto 606-8507, Japan
[4]Division of Molecular Genetics and Epigenetics, Department of Biomolecular Sciences, Faculty of Medicine, Saga University, Saga 849-8501, Japan
[5]Gladstone Institute of Cardiovascular Disease, San Francisco, CA 94158, USA
[6]Hakubi Center for Advanced Research, Kyoto University, Kyoto 606-8507, Japan
[7]PRESTO, Japan Science and Technology Agency, 4-1-8 Honcho Kawaguchi, Saitama, 332-0012, Japan
[8]These authors contributed equally to this work
*Correspondence: y-yamada@cira.kyoto-u.ac.jp
http://dx.doi.org/10.1016/j.cell.2014.01.005

SUMMARY

Cancer is believed to arise primarily through accumulation of genetic mutations. Although induced pluripotent stem cell (iPSC) generation does not require changes in genomic sequence, iPSCs acquire unlimited growth potential, a characteristic shared with cancer cells. Here, we describe a murine system in which reprogramming factor expression in vivo can be controlled temporally with doxycycline (Dox). Notably, transient expression of reprogramming factors in vivo results in tumor development in various tissues consisting of undifferentiated dysplastic cells exhibiting global changes in DNA methylation patterns. The Dox-withdrawn tumors arising in the kidney share a number of characteristics with Wilms tumor, a common pediatric kidney cancer. We also demonstrate that iPSCs derived from Dox-withdrawn kidney tumor cells give rise to nonneoplastic kidney cells in mice, proving that they have not undergone irreversible genetic transformation. These findings suggest that epigenetic regulation associated with iPSC derivation may drive development of particular types of cancer.

INTRODUCTION

Induced pluripotent stem cells (iPSCs) can be established from differentiated somatic cells by the forced induction of four transcription factors: *Oct3/4*, *Klf4*, *Sox2*, and *c-Myc* (Takahashi et al., 2007; Takahashi and Yamanaka, 2006; Maherali et al., 2007; Okita et al., 2007; Wernig et al., 2007; Woltjen et al., 2009). To achieve somatic cell reprogramming, multiple cellular processes act synergistically in a sequential manner (Brambrink et al., 2008; Polo et al., 2012; Samavarchi-Tehrani et al., 2010). Despite extensive studies, the precise mechanism of somatic cell reprogramming still remains unclear (Rais et al., 2013). It is known that non-iPSC-like colonies often appear at the intermediate stage of cellular reprogramming in vitro. In addition, there are several reports describing partial iPSCs that deviate successful reprogramming (Fussner et al., 2011; Mikkelsen et al., 2008; Sridharan et al., 2009). However, the characteristics of such failed reprogramming states are largely unknown, and no study has elucidated the failed reprogramming state from cell types other than fibroblasts.

The process of iPSC derivation shares many characteristics with cancer development. During reprogramming, somatic differentiated cells acquire the properties of self-renewal along with unlimited proliferation and exhibit global alterations of the transcriptional program, which are also critical events during carcinogenesis (Ben-Porath et al., 2008). The metabolic switch to glycolysis that occurs during somatic cell reprogramming is similarly observed in cancer development (Folmes et al., 2011). Such similarities suggest that reprogramming processes and cancer development may be partly promoted by overlapping mechanisms (Hong et al., 2009). Practically, the forced induction of the critical reprogramming factor *Oct3/4* in adult somatic cells results in dysplastic growth in epithelial tissues through the inhibition of cellular differentiation in a manner similar to that in embryonic cells (Hochedlinger et al., 2005). These studies provided a possible link between transcription-factor-mediated reprogramming and cancer development.

To elucidate the involvement of failed reprogramming in cancer development, in the present study, we generated an in vivo reprogramming mouse system using reprogramming factor-inducible alleles and examined the effects of reprogramming factor expression in somatic cells in vivo. We show that failed reprogramming-associated cells behave similarly to cancer cells

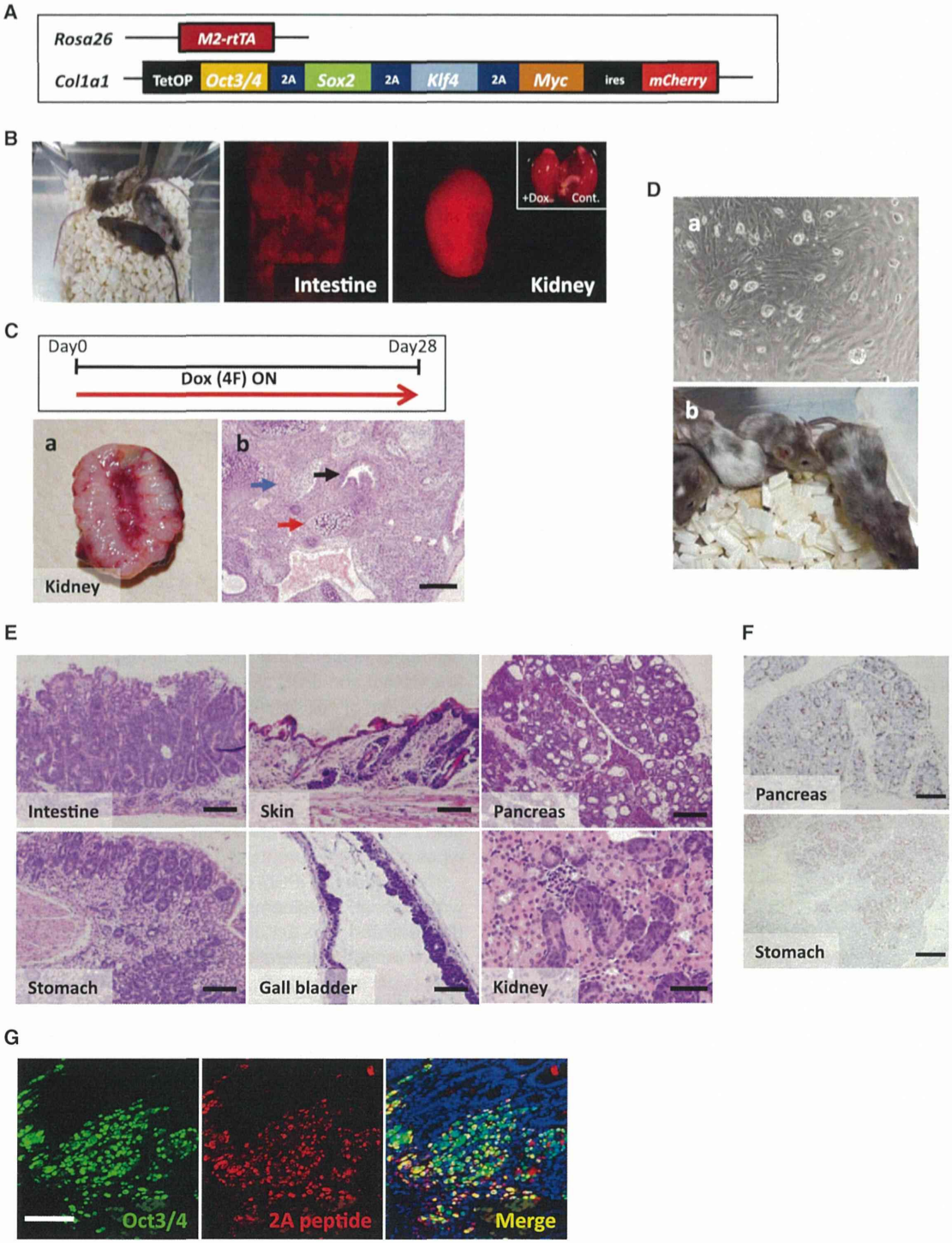

Figure 1. Reprogramming of Somatic Cells In Vivo

(A) Generation of four-factor-inducible ESCs. TetOP, tetracycline-dependent promoter.

(B) Generation of chimeric mice using OSKM-inducible ESCs. mCherry signals could be detected in various organs after Dox treatment for 3 days.

(C) Treatment of chimeric mice with Dox for 28 days resulted in the development of multiple tumors containing pluripotent stem cells. (a) A representative macroscopic image of the cut surface of the kidney tumor. (b) A histological section of the kidney tumor showing the differentiation of tumor cells into three germ layers, indicating teratoma formation. The blue, red, and black arrows represent neuronal, cartilage, and glandular epithelial components, respectively. Scale bar, 200 μm.

(legend continued on next page)

and cause neoplasia resembling Wilms tumor, a childhood blastoma in the kidney. Moreover, we demonstrate that altered epigenetic regulations cause the abnormal growth of such failed reprogramming-associated cancer cells.

RESULTS

In Vivo Reprogrammable Mouse

To establish the reprogrammable mouse system, we generated embryonic stem cells (ESCs) in which reprogramming factors can be induced under the control of doxycycline (Dox) (Figure 1A) (Carey et al., 2010; Stadtfeld et al., 2010b). We used KH2 ESCs with the optimized reverse tetracycline-dependent transactivator at the *ROSA 26* locus (Beard et al., 2006). A polycistronic cassette encoding four reprogramming factors (*Oct3/4*, *Sox2*, *Klf4*, and c-*Myc*) (Carey et al., 2010), followed by *ires-mCherry*, was targeted into the *Col1a1* gene locus under the tetracycline-dependent promoter of KH2 ESCs (Figure 1A).

Next, we generated chimeric mice via blastocyst injection of four-factor (4F)-inducible ESCs. To confirm inducible expression of the reprogramming factors and mCherry in vivo, Dox-containing water was provided to chimeric mice starting at 4 weeks of age. On day 3 of Dox treatment, we could detect the mCherry signal in various organs, including stomach, intestine, liver, pancreas, kidney, gallbladder, and skin (Figure 1B). We also confirmed the expression of reprogramming factors in germline-transmitted mouse tissues by quantitative RT-PCR (qRT-PCR) (Figure S1A available online).

Mouse embryonic fibroblasts (MEFs) containing these reprogramming factor-inducible alleles could give rise to iPSCs after Dox treatment in vitro (Figure S1B). We next asked whether responding somatic cells could be reprogrammed in vivo. The chimeric and germline-transmitted mice given Dox-containing water (2 mg/ml) from 4 weeks of age became morbid within 7–10 days and a few days, respectively. A small proportion of chimeric mice could be treated with Dox for 4 weeks, presumably because of a lower contribution of ESCs in responding tissues. Notably, mice treated with Dox for 4 weeks developed multiple tumors in several organs, such as the kidney and pancreas (Figure 1Ca), whereas tumor formation was never observed in nontreated mice (n = 7, 7 months of age). Histological analysis revealed that these tumors differentiated into three different germ layers, indicating that they are teratomas (Figure 1Cb). When teratoma cells were cultured ex vivo in the absence of Dox (no additional 4F expressions), iPSC-like cells were established (Figure 1Da). Importantly, the teratoma-derived iPSC-like cells contributed to adult chimeric mice when they were injected into blastocysts (Figure 1Db). Therefore, we conclude that somatic cells can be reprogrammed in vivo to pluripotency in our reprogrammable mouse system.

Forced Expression of Reprogramming Factors In Vivo Leads to Rapid Expansion of Dysplastic Cells

We next examined the early changes after expression of reprogramming factors in somatic cells in vivo. After treatment of 4-week-old mice with Dox for 3–9 days, all mice developed dysplastic lesions in epithelial tissues of various organs (Figure 1E), although there were variations in severity of the phenotype among chimeras. Dysplastic cells proliferated actively, as revealed by Ki67 staining (Figure 1F). Abnormal proliferation of somatic cells was observed as early as 3 days after Dox treatment (Figure S1C), and by day 7, such dysplastic cell growth was detected even for pancreatic and kidney cells, which typically do not divide actively under physiological conditions (Figures 1E and 1F). Immunofluorescent analysis of Oct3/4 and the 2A peptide (forming transgene connections) demonstrated that the dysplastic cells expressed reprogramming factors (Figure 1G). Collectively, the forced expression of reprogramming factors caused dysplastic cell expansion of epithelial tissues in vivo.

The Fate of Early Dysplastic Cells after Withdrawal of Dox

To examine whether subsequent expansion of such dysplastic cells depends on the continuous expression of reprogramming factors, we withdrew Dox for 7 days after an initial 4- to 7-day treatment (Figure 2A). Although Dox treatment for 4–7 days caused active cell proliferation in a variety of tissues of all mice, we did not observe any dysplastic cells in some mice after withdrawal of Dox (Figure 2A; Table 1). Of particular note, mice treated with Dox for periods less than 5 days before withdrawal often revealed a lack of dysplastic cells (Table 1). These data suggest that early dysplastic cell growth requires continuous expression of reprogramming factors. We next investigated the fate of eliminated dysplastic proliferating cells after the withdrawal of Dox. Bromodeoxyuridine (BrdU) was injected into mice during Dox treatment to label proliferating cells caused by reprogramming factor expression during the first 7 days (Hochedlinger et al., 2005), and then mice were sacrificed after the withdrawal of Dox for 7 days, on day14. Notably, BrdU-labeled cells were often observed in normal-looking pancreatic and kidney tissues at day14 (Figure 2B). Furthermore, BrdU-labeled cells in the pancreatic islets also expressed insulin (Figure 2B). This suggests that the expanded cells caused by the transient expression of reprogramming factors were, at least in part, integrated into normal-looking tissues after Dox withdrawal.

(D) Teratomas contain pluripotent stem cells. (a) Ex vivo teratoma culture gave rise to iPSC-like colonies without Dox exposure. (b) Teratoma-derived iPSCs contributed to adult chimeric mice.

(E) Dysplastic cell expansion by the forced expression of reprogramming factors in vivo. The histology of various organs of mice treated with Dox for 3 to 9 days. Scale bars, 200 μm (intestine, skin, pancreas, stomach, and gall bladder) and 100 μm (kidney).

(F) Ki67 immunostaining revealed active proliferation of the dysplastic cells in the pancreas and stomach. Scale bars, 200 μm.

(G) Immunofluorescent staining for Oct3/4 and 2A peptide in the intestine of an OSKM chimeric mouse treated with Dox for 7 days. The 2A antibody used here recognizes both Oct3/4-P2A and Sox2-T2A. Dysplastic cells showed positive staining for both Oct3/4 and 2A. Scale bar, 50 μm.

See also Figure S1.

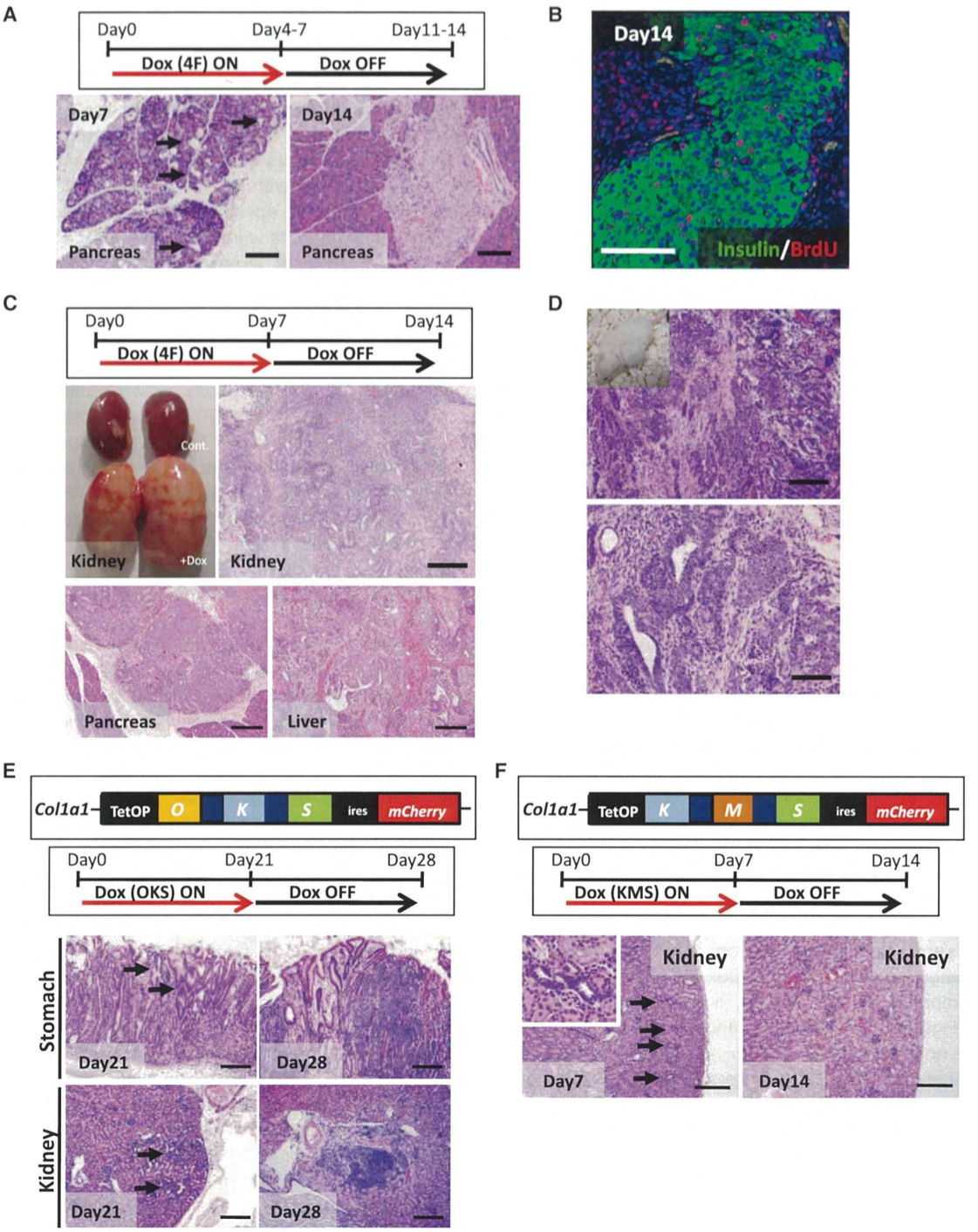

Figure 2. Transient Expression of Reprogramming Factors Causes Neoplasia

(A) A schematic drawing of the experiment and histological sections of the pancreas taken on days 7 and 14. Dysplastic cell growth was induced by treatment with Dox for 7 days (arrows on day 7). The pancreatic section taken on day 14 revealed normal histology. Scale bars, 200 μm.

(B) Double immunofluorescence for insulin and BrdU in the pancreas on day 14. For the pulse and chase experiment, BrdU was injected intraperitoneally every day during Dox administration starting on day 2 (days 2–7), followed by withdrawal of Dox for 7 days. BrdU-positive cells were frequently observed in normal-looking pancreatic islet cells, which also expressed insulin. Scale bar, 100 μm.

(C) Treatment of OSKM chimeric mice with Dox for 7 days, followed by the withdrawal of Dox for another 7 days. The macroscopic image shows the development of bilateral kidney tumors on day 14. Representative histological images are shown for Dox-withdrawn tumors in the kidney, pancreas, and liver. Scale bars, 200 μm.

(legend continued on next page)

Table1. Transient Expression of Reprogramming Factors Causes Tumor Development

		Kidney		Pancreas		Liver	
Dox Treatment	n	No Phenotype	Dysplastic Growth	No Phenotype	Dysplastic Growth	No Phenotype	Dysplastic Growth
4 days ON→OFF	4	2	2	4	0	3	1
5 days ON→OFF	2	1	1	2	0	2	0
6 days ON→OFF	5	1	4	2	3	3	2
7 days ON→OFF	33	7	26	22	11	25	8

Prolonged Expression of Reprogramming Factors Leads to Transgene-Independent Tumor Formation in Somatic Cells

In contrast to the reversion of early dysplastic proliferating cells into normal-looking cells, mice that had been given Dox for 7 days often went on to develop tumors in multiple responding organs even after Dox withdrawal (Figure 2C; Table 1). The developed tumors consisted of histologically undifferentiated dysplastic cells, which were distinct from teratoma cells (Figures 2C and S2A). The dysplastic cells invaded the surrounding tissues, which is one of the hallmarks of cancer cell growth (Figure S2A). Dox-withdrawn tumor cells were negative for 2A staining, affirming that they grew independent of transgene expression (Figure S2B). Dox-withdrawn kidney tumors were similarly observed in elderly mice given Dox starting at 14 weeks of age (13 out of 19 mice). When Dox-withdrawn kidney tumor cells were transplanted into the subcutaneous tissues of immunocompromised mice, they formed secondary tumors within 3 weeks without Dox administration (Figures 2D and S2C), reflecting the neoplastic potential of Dox-withdrawn tumor cells.

Reprogramming factors in our transgenic system include *c-Myc*, a well-known oncogene. To investigate the contribution of *c-Myc* on the development of Dox-withdrawn tumors, we generated three-factor-inducible chimeric mice, which express *Oct3/4*, *Sox2*, and *Klf4* (OKS), but not *c-Myc*, by the targeted insertion of transgenes into the identical locus as 4F (OSKM)-inducible mice (Figure 2E). Similar to 4F-induced mice, OKS induction in vivo caused dysplastic cell growth in various organs yet required longer periods of treatment (Figure 2E). After 3 weeks of induction of OKS followed by withdrawal for 7 days, these mice developed the Dox-withdrawn tumors consisting of undifferentiated dysplastic cells in multiple organs (4 out of 8 mice; Figure 2E). Therefore, transgenic *c-Myc* is dispensable for the development of Dox-withdrawn tumors.

Oct3/4 plays a critical role in cellular reprogramming, and expression of three factors (*Klf4*, *c-Myc*, and *Sox2*) in the absence of *Oct3/4* is not sufficient for iPSC generation (Takahashi and Yamanaka, 2006). To further demonstrate a link between cellular reprogramming and Dox-withdrawn tumor development, we generated chimeric mice in which *Klf4*, c-*Myc*, and *Sox2* (KMS), but not *Oct3/4*, can be induced upon Dox treatment (Figure 2F). Following Dox treatment for 7 days, we observed dysplastic cell growth in the kidney of KMS-inducible mice (three out of six mice; Figure 2F). However, in sharp contrast to OSKM/OKS-induced mice, the withdrawal of Dox eliminated the dysplastic cells in the kidney of KMS-induced mice (n = 17; Figure 2F). A previous study demonstrated that ectopic expression of *Oct3/4* alone can induce dysplastic growth whereas the transgene withdrawal leads to complete reversion of such dysplasia (Hochedlinger et al., 2005). Consistent with the previous observation, the *Oct3/4*-single induction under the same experimental condition failed to form Dox-withdrawn tumors (n = 18; Figure S2D). Taken together, we conclude that reprogramming pressure toward pluripotency driven by the combination of reprogramming factors is associated with the development of Dox-withdrawn tumors.

Loss of Cell Identity and Gain of ESC-Related Gene Expression in Dox-Withdrawn Tumors

To characterize Dox-withdrawn tumor cells, we examined gene expression in kidney tumors that arose in OSKM-inducible mice treated with the 7+/7− Dox regimen. In the KH2 system, transgene expression in the kidney is induced exclusively in the tubule cells (Beard et al., 2006). We observed decreased expression of kidney tubule cell-specific genes in Dox-withdrawn kidney tumors, indicating loss of kidney cell identity (Figure 3A). A previous study dissected the gene expression signature of ESCs into three functional modules: core pluripotency factors, Polycomb complex factors, and Myc-related factors (Kim et al., 2010). Notably, microarray analysis revealed that the ESC-Core module is similarly activated in Dox-withdrawn kidney tumors and ESCs (Figure 3B) (Ohta et al., 2013). We also found that the Myc module displays similar activation between Dox-withdrawn tumors and ESCs (Figure S3A). The activation of ESC-Core and ESC-Myc modules was similarly confirmed in transplanted secondary tumors (Figure S3B).

(D) Minced Dox-withdrawn tumor cells were injected in the subcutaneous tissues of immunocompromised mice. A histological section of one of the tumors phenocopied the original Dox-withdrawn tumor. Scale bars, 200 μm (upper panel) and 100 μm (lower panel).

(E) A schematic drawing of the OKS transgene at the *Col1a1* locus. A histological section of the kidney on days 21 and 28. The expansion of dysplastic cells was observed in the stomach and kidneys on day 21 (arrows). The dysplastic cell growth could be detected even after the withdrawal of Dox in OKS-induced mice (day 28). Scale bars, 200 μm.

(F) A schematic drawing of the KMS transgene. A histological section of a kidney after the treatment with Dox for 7 days (day 7) and the withdrawal of Dox for another 7 days (day 14). KMS induction leads to dysplastic growth in the kidney tubule cells (arrows for day 7). The inset shows a higher-magnification image. No dysplastic cells were detectable in the kidneys of KMS-induced mice after the withdrawal of Dox (day 14). Scale bars, 200 μm.

See also Figure S2.

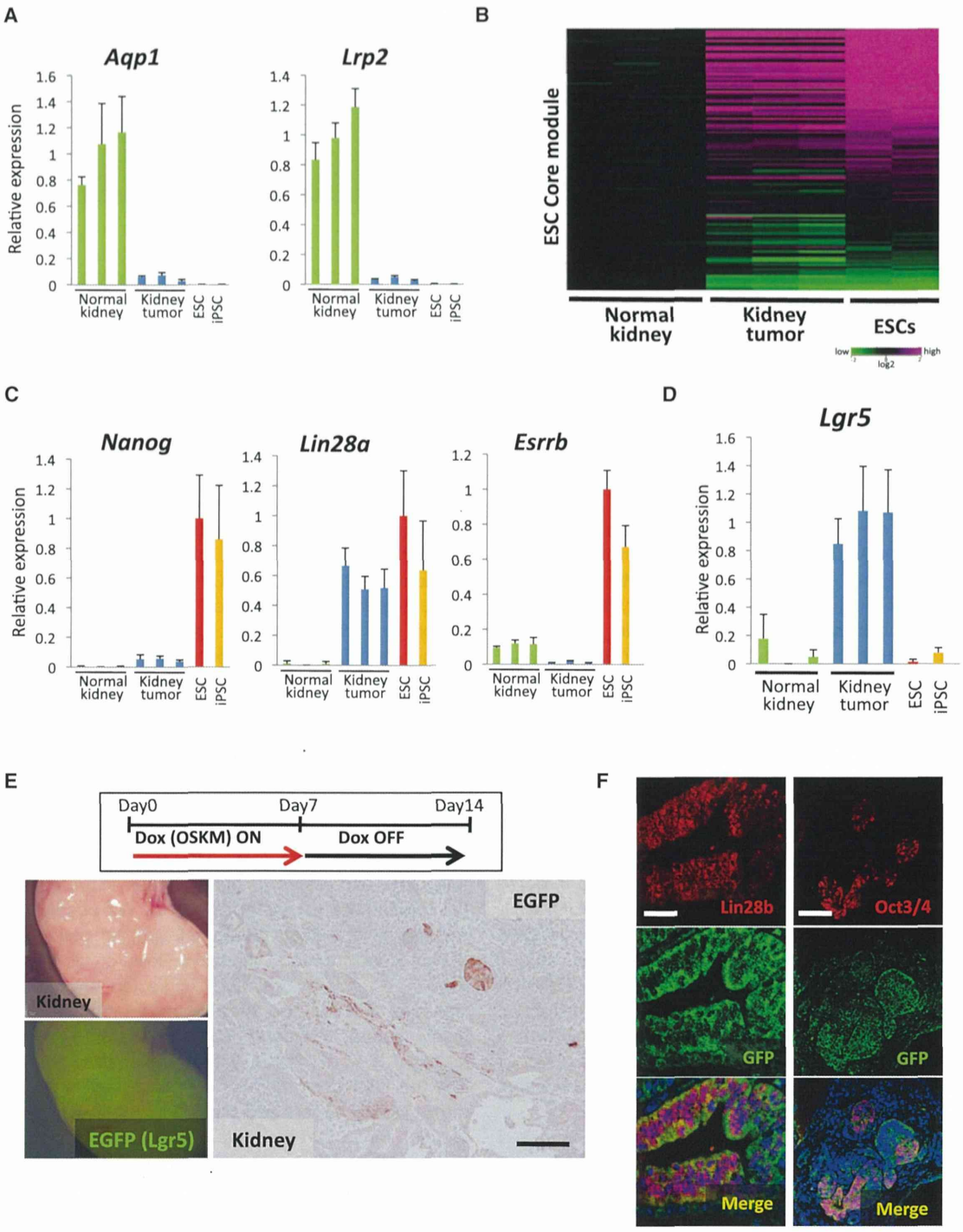

Figure 3. Loss of Cell Identity and Gain of ESC-Related Gene Expression in the Dox-Withdrawn Tumors

(A) The results of the qRT-PCR analyses of *Aqp1* and *Lrp2*. The expression levels of *Aqp1* and *Lrp2* were significantly downregulated in the Dox-withdrawn kidney tumors. Data are presented as mean ± SD. The mean level of normal kidney samples was set to 1.

(B) The microarray analyses revealed the activation of the ESC Core module in Dox-withdrawn kidney tumors.

(C) The results of the qRT-PCR analyses of pluripotency-related genes. Data are presented as mean ± SD. The transcript level in ESCs was set to 1.

(D) *Lgr5* as a candidate marker of Dox-withdrawn kidney tumor cells. *Lgr5* was specifically expressed in Dox-withdrawn kidney tumors. Data are presented as mean ± SD. The mean level of kidney tumors was set to 1.

(E) A schematic drawing of the experimental protocol using chimeric mice with both reprogrammable alleles and the *Lgr5-EGFP* allele. Macroscopic images of the Dox-withdrawn kidney tumor with the *Lgr5-EGFP* allele showing scattered EGFP signals in the kidney tumor. GFP immunostaining of kidney tumor sections revealed that the GFP signals are detectable specifically in tumor cells. Scale bar, 100 μm.

(legend continued on next page)

Some pluripotency-related genes, including *Nanog*, *Oct3/4*, and *Lin28a*, were upregulated in the Dox-withdrawn kidney tumor cells as compared to normal kidney tissue, although the expression levels of both *Nanog* and endogenous *Oct3/4* were significantly lower than that of pluripotent stem cells (Figures 3C and S3C). Conversely, other pluripotency-related genes, such as *Esrrb*, were not upregulated in these tumors (Figures 3C).

To further characterize Dox-withdrawn tumor cells, we sought to identify tumor-cell-specific markers. We found that *Lgr5* is specifically upregulated in Dox-withdrawn kidney tumor cells, but not in adult kidney tissues or pluripotent stem cells (Figure 3D). Increased expression of *Lgr5* was similarly observed in the transplanted secondary tumors (Figure S3D). Therefore, we established iPSC lines from OSKM-inducible MEFs containing *Lgr5-EGFP* reporter allele in which *Lgr5* expression can be visualized by enhanced green fluorescent protein (EGFP) (Barker et al., 2007). The established *Lgr5*-reporter iPSCs do not express EGFP in ESC culture conditions (Figure S3E). OSKM-inducible *Lgr5* reporter chimeric mice at 4 weeks of age were treated with the 7+/7− Dox regimen. Again, these mice developed Dox-withdrawn kidney tumors consisting of dysplastic cells (Figure 3E). The scattered EGFP signals were observed in kidney tumors (Figure 3E), and immunohistochemical analysis revealed that *Lgr5* is specifically expressed in part of Dox-withdrawn kidney tumor cells (Figures 3E and S3E). These findings indicate that Dox-withdrawn kidney tumors contain *Lgr5*-positive cells and that the *Lgr5* reporter allele is available to specifically identify the Dox-withdrawn kidney tumor cells that are distinct from fully reprogrammed pluripotent stem cells. Of note, some of the *Lgr5*-expressing tumor cells also expressed Oct3/4 and Lin28b in immunohistochemical analysis (Figures 3F and S3F), thus suggesting that *Lgr5*-expressing tumor cells share some characteristics with pluripotent stem cells. The fact that Dox treatment for longer than 8 days followed by Dox withdrawal often results in teratoma formation supports the notion that partial reprogramming toward pluripotent stem cells is involved in the development of Dox-withdrawn tumors (data not shown). Altogether, our findings indicate that *Lgr5*-expressing tumor cells are distinct from pluripotent stem cells but contain partially reprogrammed cells.

Failed Repression of ESC-Polycomb Targets in Dox-Withdrawn Tumors

In contrast to ESC-like activation observed for both the ESC-Core and ESC-Myc modules, the ESC Polycomb repressive complex (PRC) module was differentially expressed between Dox-withdrawn tumors and ESCs (Figure 4A). We found that a number of ESC-PRC targeted genes are not repressed in both kidney tumors and transplanted secondary tumors (Figures 4A, S4A, and S4B), indicating that the failed repression of ESC-PRC targets is associated with the development of Dox-withdrawn tumors. Consistent with the notion, more than one-forth of the upregulated genes in tumor cells as compared to ESCs (greater than 3-fold upregulation) were targets of PRC in ESCs (Mikkelsen et al., 2007) (Table S1). We also found that Dox-withdrawn kidney tumors express kidney-precursor-expressing genes such as *Six2*, *Eya1*, and *Lgr5* (Barker et al., 2012; Kobayashi et al., 2008) (Figures 4B and S4C). In particular, *Six2* and *Lgr5*, which are also PRC targets in ESCs (Mikkelsen et al., 2007), are specifically upregulated in both Dox-withdrawn kidney tumors and secondary tumors when compared to both normal kidney tissues and pluripotent stem cells (Figures 3D, 4B, S3D, and S4D). Chromatin immunoprecipitation (ChIP)-qPCR experiments confirmed decreased H3K27me3 levels at both *Six2* and *Lgr5* promoter regions in Dox-withdrawn tumors when compared with those in normal kidney tissues (Figure S4E). Failed repression of the ESC-PRC module was also detectable in unsuccessfully reprogrammed kidney cells in vitro, which were established by the transient expression of reprogramming factors in isolated kidney tubule cells in vitro (Figure S4F).

We next examined the kinetics of transcriptional changes during the development of the Dox-withdrawn tumors. Immunohistochemical analysis revealed that early dysplastic cells at day 7 coincide with transgene-expressing cells (Figure S4G). Taking advantage of florescence-linked transgene expression in our mice, we fluorescence-activated cell sorted mCherry-positive kidney cells in OSKM mice given Dox for 7 days (D7), isolating early dysplastic cells for gene expression analysis. Fluorescence-activated cell-sorted D7 LacZ-mCherry-expressing kidney cells were used as a control (Figure S4H). Decreased expression of proximal tubule cell markers was observed in the D7 OSKM cells as compared to D7 LacZ cells, suggesting that the loss of kidney cell identity occurs in early dysplastic cells (Figure S4I). In contrast, increased expression of ectopic stem/progenitor cell markers was not evident in D7 OSKM cells (Figure S4I). These findings suggest that remodeling of global transcriptional profiles toward a stem/progenitor-like state is specifically associated with transgene-independent, late dysplastic cells.

To investigate cell-of-origin effects on failed reprogramming, we next performed a microarray analysis for Dox-withdrawn liver tumors and compared the data with that of kidney tumors. As observed in kidney tumors, the liver tumors displayed failed repression of the ESC-PRC module, accompanied by activation of both the ESC-Core and Myc modules (Figure S4J; Table S1). Although derepressed PRC module genes in kidney tumors and liver tumors often overlapped (Figure S5A; Table S1), we found differentially derepressed PRC genes between kidney and liver tumors. Notably, such differentially derepressed PRC genes were associated with kidney and liver development, respectively. These findings suggest that failed PRC repression in Dox-withdrawn tumors may be associated with the activation of a developmental transcription

(F) Dox-withdrawn tumors express pluripotency-related proteins. Double immunofluorescence for Lin28b and GFP (Lgr5) revealed that the GFP-positive tumor cells also expressed Lin28b. Double immunofluorescence for Oct3/4 and GFP (Lgr5) showed that a subset of GFP-positive tumor cells expressed Oct3/4 in the nucleus. Scale bars, 20 μm.
See also Figure S3.

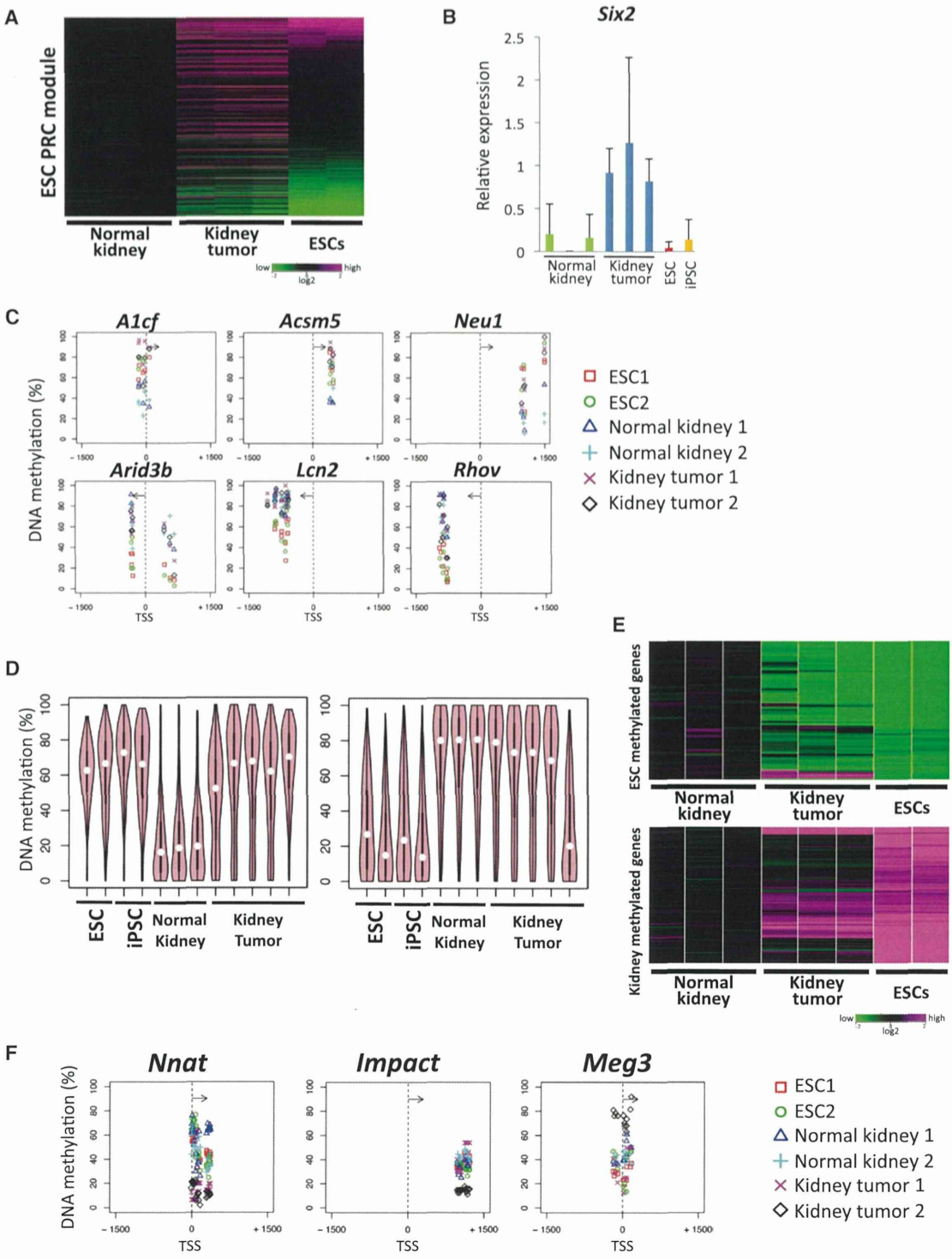

Figure 4. Altered Epigenetic Regulation in Dox-Withdrawn Tumors

(A) The microarray analyses revealed that ESC-PRC target genes were often activated in Dox-withdrawn kidney tumors compared to normal kidney tissues.

(B) *Six2* was highly expressed only in the Dox-withdrawn kidney tumors. Data are presented as mean ± SD. The mean level of kidney tumors was set to 1.

(C) Altered DNA methylation patterns in Dox-withdrawn tumors and the DNA methylation status of representative genes in the RRBS analyses.

(D) The global analyses for the DNA methylation levels. Genes that were differentially methylated between ESCs and normal kidney samples (more than 30% difference) were extracted and then analyzed for DNA methylation levels in Dox-withdrawn kidney tumors. Kidney tumors gain DNA methylation at ESC-methylated genes, whereas kidney-methylated genes often retain their methylation status in kidney tumors.

(legend continued on next page)

program, which is affected in part by the cell of origin (Figure S5A).

Altered DNA Methylation in Dox-Withdrawn Kidney Tumor Cells

Somatic cell reprogramming is accompanied by global changes in DNA methylation patterns (Mikkelsen et al., 2008). The fact that failed reprogramming can cause tumor development suggests that altered epigenetic modifications play a role in tumorigenesis. To quantitatively profile DNA methylation in Dox-withdrawn tumors, we next performed reduced representation bisulfite sequencing (RRBS) (Meissner et al., 2005). We identified a number of genes with altered DNA methylation levels in Dox-withdrawn tumors as compared to normal kidney tissues. Dox-withdrawn tumors revealed frequent gains of DNA methylation at DNA-methylated genes in ESCs, whereas loss of methylation at DNA-methylated genes in kidney tissues was not evident (Figure 4C). To validate these findings, we next performed a global analysis. We first extracted genes differentially methylated between ESCs and normal kidney samples and then examined their DNA methylation in Dox-withdrawn tumors. The global analysis confirmed that Dox-withdrawn kidney tumors gained de novo methylation at ESC-methylated genes, whereas kidney-methylated genes often retain their methylation in Dox-withdrawn kidney tumors (Figure 4D). Consistent with these findings, ESC-methylated genes were frequently found to be repressed in Dox-withdrawn tumors, whereas kidney-methylated genes tended to remain silent in these tumors (Figure 4E). These results suggest that loss of somatic cell-specific DNA methylation is preceded by a gain of ESC-specific DNA methylation patterns during the reprogramming process.

Adult cancers generally exhibit two distinct patterns of alterations in DNA methylation: site-specific DNA hypermethylation and global DNA hypomethylation (Jones and Baylin, 2002; Yamada et al., 2005). We performed specified regional analyses for the DNA methylation in normal kidney tissues and Dox-withdrawn kidney tumors. DNA hypermethylation at promoter regions in Dox-withdrawn tumors was not detectable, regardless of the presence of CpG islands (Figure S5B). Additionally, decreased DNA methylation levels at intergenic regions were not obvious in Dox-withdrawn tumors (Figure S5B).

We found that Dox-withdrawn kidney tumors aberrantly express a number of imprinted genes and that altered expression levels are similar to those in ESCs (Figure S5C). When DNA methylation status at differentially methylated regions (DMRs) of imprinted genes were examined in Dox-withdrawn tumors using a MassARRAY platform (Ehrich et al., 2005), we found frequent alterations of DNA methylation status at DMRs in Dox-withdrawn tumors (Figure S5D). The aberrant genomic methylation levels at imprinted genes in Dox-withdrawn tumors were also confirmed by RRBS analysis (Figures 4F and S5E). Intriguingly, each Dox-withdrawn tumor revealed variable aberrations in DNA methylation at different imprinted genes. The aberrant methylation includes hypermethylation at the *Meg3* (*Gtl2*) DMR, which has been correlated with impaired differentiation properties of iPSCs (Stadtfeld et al., 2010a) (Figures 4F and S5E). Moreover, SNP analysis in the hybrid KH2 background revealed that the altered expression of some imprinted genes in Dox-withdrawn tumors arise from biallelic transcription, compared to monoallelic expression in the original OSKM-inducible ESCs (Figure S5F). Collectively, these results suggest that genomic imprinting is unstable in Dox-withdrawn tumors and provide additional evidence that altered gene expression underlying tumor development is associated with altered epigenetic signatures.

Dox-Withdrawn Kidney Tumors Resemble Wilms Tumors

Histological analysis revealed that Dox-withdrawn kidney tumors in reprogrammable mice resemble Wilms tumor, the most common pediatric kidney cancer (Figure 5A). A number of studies demonstrated that increased expression of *Igf2* with DNA hypermethylation at the *H19* DMR is one of the causative and most common alterations in Wilms tumors (Ogawa et al., 1993; Steenman et al., 1994). We confirmed that Dox-withdrawn tumors express a significantly higher level of *Igf2* than noninduced tissues (Figures 5B and S6A). Moreover, consistent with altered DNA methylation at other imprinted genes, the increased methylation at the *H19* DMR was detectable in some Dox-withdrawn kidney tumors (Figure 5C).

To additionally evaluate the similarity between Dox-withdrawn kidney tumors and Wilms tumors, we next compared global gene expression patterns. We first selected genes that are upregulated more than 5-fold in Dox-withdrawn kidney tumors in comparison with noninduced kidney tissues and then assessed expression of their human orthologs in human normal kidney tissues, Wilms tumors, and human ESCs (hESCs) using previously reported microarray data sets (Tchieu et al., 2010; Yusenko et al., 2009). We found that upregulated genes in Dox-withdrawn kidney tumors are frequently upregulated in both Wilms tumors and hESCs as compared to normal kidney samples (Figure 5D), whereas this upregulation is not evident in adult kidney cancers (renal cell carcinomas [RCCs]) (Figure S6B).

We also analyzed the expression of genes in ESC-Core, ESC-Myc, and ESC-PRC modules in Wilms tumors. Notably, ESC-upregulated genes in both ESC-Core and ESC-Myc modules are similarly activated in Wilms tumors (Figures 5D and S6C), although *NANOG* and *OCT3/4* are not expressed in Wilms tumors. In contrast, a fraction of ESC-PRC targeted genes expressed in kidney progenitors, such as *SIX2* and *LGR5*, are specifically upregulated in Wilms tumors as compared with

(E) DNA-methylation-associated gene regulation in Dox-withdrawn tumors. The vast majority of ESC-methylated genes were downregulated in Dox-withdrawn tumors, whereas a significant portion of kidney-methylated genes remained repressed in these tumors. ESC-methylated genes with decreased expression levels in ESCs and kidney-methylated genes with decreased expression levels in the kidney tissues were examined.

(F) Altered DNA methylation at the DMR of imprinting genes. Note that kidney tumor 2 showed aberrant methylation patterns at *Nnat*, *Impact*, and *Meg3*. In contrast, kidney tumor 1 showed an aberration only at *Nnat*.

See also Figures S4 and S5.

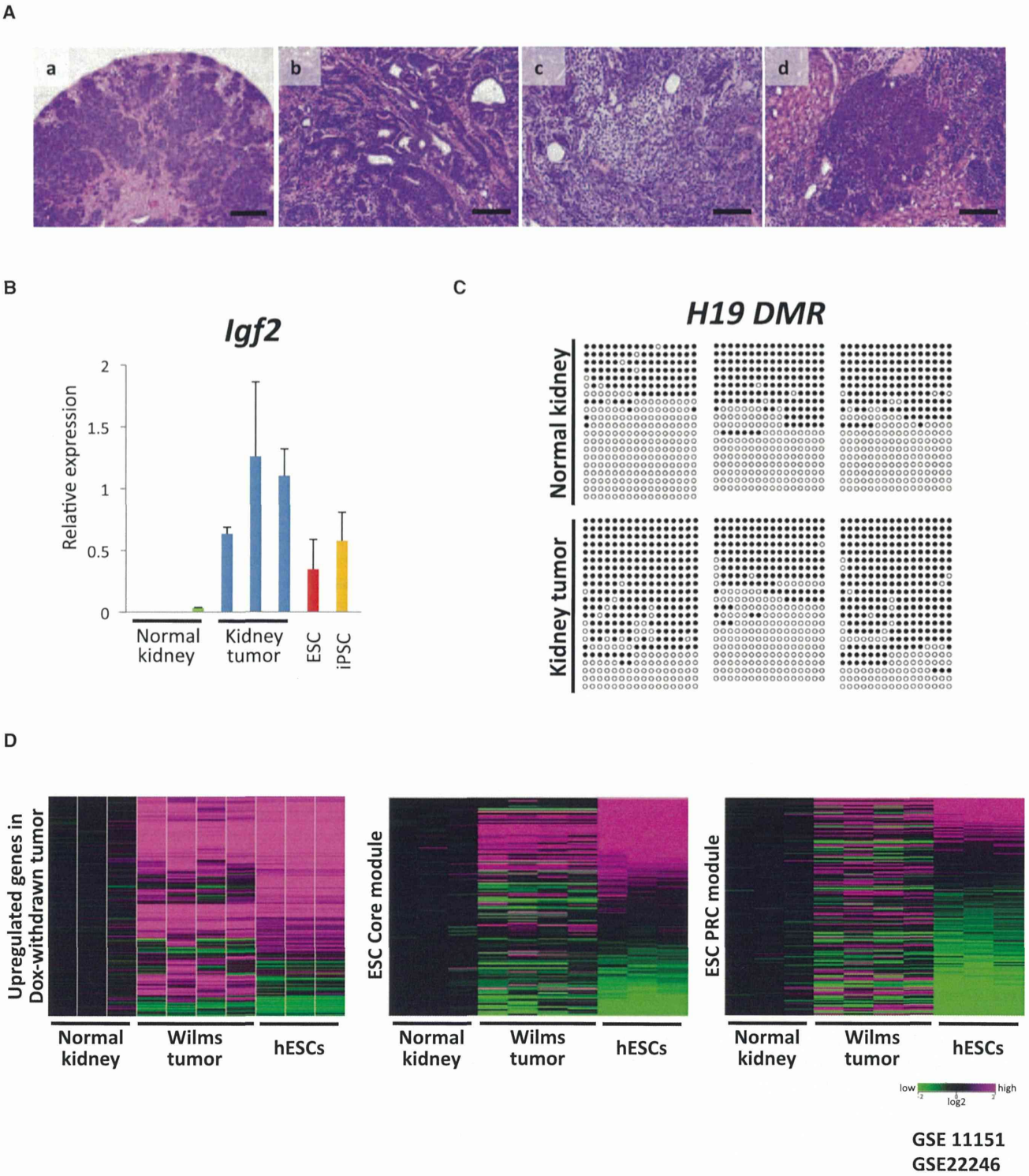

Figure 5. Dox-Withdrawn Kidney Tumors Resemble Wilms Tumors

(A) Representative histological findings of Dox-withdrawn kidney tumors (a–d). Tumors consisted of epithelial (b), stromal (c), and blastema-like (d) compartments, which are histological features of Wilms tumors. Scale bars, 500 μm (a) and 100 μm (b–d).

(B) The results of the qRT-PCR analysis for *Igf2*. *Igf2* was highly expressed in Dox-withdrawn kidney tumors. Data are presented as mean ± SD. The mean level of kidney tumors was set to 1.

(legend continued on next page)

those in normal kidney tissues, hESCs, and RCCs (Figures 5D and S6D) (Aiden et al., 2010). Collectively, kidney tumors induced by the transient expression of reprogramming factors display a number of shared characteristics with Wilms tumor. These findings also indicate that our mouse model may prove useful to uncover the pathogenesis of Wilms tumors.

iPSCs Derived from Dox-Withdrawn Kidney Tumors Contribute to Nonneoplastic Kidney Tissues in Chimeric Mice

We next tried to establish iPSCs from Dox-withdrawn kidney tumor cells. The tumor cell-specific *Lgr5-EGFP* reporter allele defined in this study was utilized to isolate tumor cells (Figures 3D, 3E, and S3E). *Lgr5*-expressing GFP-positive tumor cells were sorted and cultured in vitro with Dox to establish iPSCs from tumor cells (Figure 6A). During the culture of *Lgr5*-expressing tumor cells in vitro, *Nanog* expression at a level comparable to that in pluripotent stem cells was detected as early as 7 days after reprogramming factor induction (Figure 6B), a rate faster than the reprogramming process from normal kidney tubule cells in vitro (Figure S7A). After 2 weeks of culture with Dox exposure, more than 20 alkaline phosphatase (AP)-positive iPSC-like colonies were obtained from 100 *Lgr5*-expressing tumor cells (Figure S7B). We were able to establish Dox-independent iPSC lines from tumor cells at 3 weeks after transgene induction (Figure 6C), suggesting that the Dox-withdrawn tumor cells can be readily reprogrammed into pluripotent stem cells.

Cancers are believed to arise through the accumulation of multiple genetic abnormalities. We next investigated whether genetic abnormalities mandate the emergence of in Dox-withdrawn tumors. Exonic regions of 514 genes that include human-cancer-related genes in transplanted secondary kidney tumors were sequenced using a hybridization selection technique combined with next-generation sequencing (Table S3). Mutations in *Wt1*, *Wtx*, *Ctnnb1*, and *Trp53*, all of which have been identified in a subset of Wilms tumors, were not detected in three tumors examined. In addition, no cancer-related gene mutations were enriched in these tumors (data not shown). Array-based comparative genomic hybridization (CGH) revealed no prevalent chromosomal alteration in tumor samples (Figure S7C).

Finally, we injected the tumor-derived iPSCs into blastocysts to generate chimeric mice. Tumor-derived iPSCs contributed into adult chimeric mice (Figure 6D). Notably, the kidney-tumor-derived iPSCs differentiated into normal-looking kidney tissues (Figures 6E, 6F, and S7D). Moreover, these chimeric mice did not develop tumors even at 24 weeks of age (n = 8). To further demonstrate that tumorigenic cells can be reprogrammed into nonneoplastic cells, we also established iPSCs from the transplanted secondary tumors and confirmed their contribution to nonneoplastic kidney tissues (Figure S7E). These results substantiate that a genetic context of the Dox-withdrawn kidney tumor cells is not determinant of the cancer phenotype and support the conclusion that altered epigenetic regulations cause the abnormal growth in somatic cells, leading to the development of Dox-withdrawn tumors.

DISCUSSION

During somatic cell reprogramming, iPSCs gain the capacity for unlimited growth without particular genetic alterations. Using abbreviated reprogramming factor expression in vivo, we demonstrate that transient expression of reprogramming factors leads to tumor development. Such tumors display altered epigenetic modifications, indicating that epigenetic regulation characteristic of cellular reprogramming may also confer neoplastic growth properties to somatic cells. Intriguingly, Dox-withdrawn tumor cells are readily reprogrammed into pluripotent stem cells by additional 4F expression, indicating that the tumor cells represent a cellular state closer to iPSCs than the original somatic cells. Moreover, kidney tumor cell-derived iPSCs contribute to various somatic cell types and give rise to nonneoplastic kidney cells in mice. These data demonstrate that the abnormal growth of unsuccessfully reprogrammed cells depends predominantly on epigenetic regulations and raise the possibility that particular types of cancer may arise exclusively through altered epigenetic regulation.

Histological features of Dox-withdrawn tumors imply that unsuccessfully reprogrammed cells lack the ability to terminal differentiate along multiple lineages. It is noteworthy that Dox-withdrawn tumor cells fail to repress ESC-PRC targets yet share the activation of ESC core regulatory circuitry and Myc-related genes with pluripotent stem cells. It is conceivable that the repression of ESC-PRC targets would be exclusively associated with the acquisition of pluripotency, whereas activation of ESC core regulatory circuitry and Myc targets lead to self-renewing activity. This notion is also consistent with previous findings that PRC components are important for successful reprogramming in humans (Onder et al., 2012). Notably, the failed repression of the ESC-PRC module was detectable in previously reported partially reprogrammed cells in vitro (Polo et al., 2012), in which the activation of both ESC-Core and ESC-Myc modules had already occurred (Figure S7F). We also found that unsuccessfully reprogrammed kidney cells tend to retain DNA methylation at kidney-specific methylated genes. Considering that global epigenetic reorganization, including changes in both H3K27 methylation and DNA methylation, occurs during the later phase of iPSC generation (Polo et al., 2012), the expected repression of ESC-PRC targets and demethylation of somatic cell-specific genomic methylation might play a role in the final stages of successful somatic cell reprogramming.

Recently, Abad et al. reported that in vivo reprogramming allows the acquisition of totipotent features resulting in embryo-like cyst formation in reprogrammable mice (Abad et al., 2013). However, in the present study, we did not observe such cystic structures in Dox-treated reprogrammable mice.

(C) The bisulfite sequencing analysis revealed increased DNA methylation levels at the *H19* DMR containing two CTCF binding sites in Dox-withdrawn tumors.
(D) The results of the global expression analyses in Wilms tumors. The human orthologs of upregulated genes in Dox-withdrawn tumors and ESC module genes were assessed using previously reported microarray data sets (GSE11151 and GSE22246).
See also Figure S6.

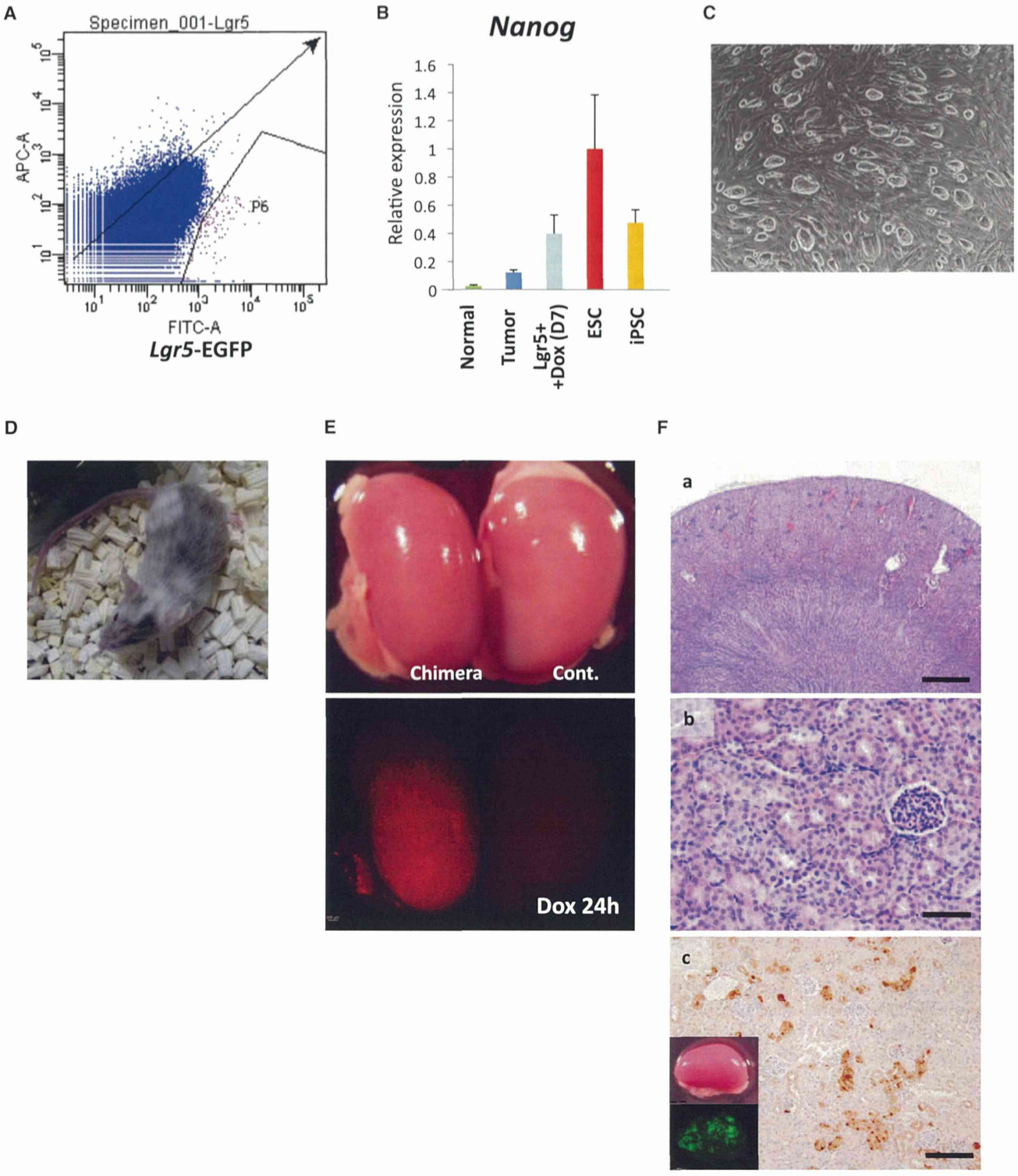

Figure 6. Generation of iPSCs from Dox-Withdrawn Tumors and Their Contribution to Normal-Looking Kidney Tissue

(A) The fluorescence-activated cell sorting analyses of Dox-withdrawn kidney tumor cells in a reprogrammable chimeric mouse with the *Lgr5*-EGFP reporter. GFP-positive *Lgr5*-expressing cells were sorted to exclusively isolate Dox-withdrawn tumor cells.

(B) Dox treatment of *Lgr5*-expressing tumor cells caused the rapid induction of *Nanog*. The *Nanog* levels were examined after seven days of treatment with Dox in vitro. Data are presented as mean ± SD. The level in ESCs was set to 1.

(C) An image of iPSCs derived from *Lgr5*-positive kidney tumor cells.

(legend continued on next page)

Furthermore, teratoma-derived in vivo iPSCs in this study failed to differentiate into placental tissues despite robust fetal contribution upon injection into eight-cell-stage embryos (data not shown), suggesting that not all in vivo iPSCs are totipotent. Because the previous study was conducted using circulating iPSCs recovered in blood, the cell of origin for in vivo reprogramming might affect the acquisition of totipotent features. It should be also noted that Abad et al. utilized germline-transmitted transgenic mice that harbor lentivirus-mediated integration of inducible reprogramming factors (Carey et al., 2009) whereas we examined chimeric mice with transgenes at a targeted locus. The different levels of transgene induction caused by such distinct transgenic systems may underlie differences in the phenotypes observed between these two studies.

Here, we show that failed reprogramming-associated cancers resemble Wilms tumors in terms of histology and molecular characteristics, including aberrant expression of imprinted genes correlated with altered DNA methylation. It is well known that Wilms tumors have characteristics distinct from adult kidney cancers in many aspects. On the basis of our findings in Dox-withdrawn tumors, we discovered that Wilms tumors harbor an activated ESC core regulatory circuitry. This is in sharp contrast to previous findings that most adult cancers do not show activation of ESC core regulatory circuitry (Kim et al., 2010). We also found that many ESC-PRC targets are not repressed in Wilms tumors, despite common repression in many cancers (Ben-Porath et al., 2008; Kim et al., 2010). Gene Ontology analysis revealed that derepressed PRC genes in Wilms tumors include genes involved in kidney development, whereas they are not enriched in derepressed PRC genes in RCCs (data not shown), suggesting that activation of the embryonic kidney transcriptional network is associated with Wilms tumor development. Taken together, strongly active ESC-core regulatory circuitry and derepression of certain ESC-PRC targets may characterize Wilms tumors and may account for the characteristics distinctive of Wilms tumors and adult kidney cancers.

Although we revealed striking similarity between Dox-withdrawn kidney tumors and Wilms tumors, it remains unclear whether reprogramming processes play a role in the development of human Wilms tumors. It has been widely accepted that nephrogenic rests, abnormally persistent clusters of embryonal cells, are the precursors of Wilms tumors. Considering the artificial expression of reprogramming factors in our experimental system, the current study does not provide direct evidence that dedifferentiation is normally involved in the human Wilms tumor development. Yet, based on our findings, it is conceivable that a reprogramming process might cause cell-fate conversion into progenitor-like states, leading to the development of nephrogenic rests required for the early stages of Wilms tumorigenesis. Further detailed analyses using human samples are required to uncover the role of reprogramming in cancer development in humans.

In summary, we demonstrated that premature termination of in vivo reprogramming causes tumor development resembling Wilms tumor. Our findings suggest that altered epigenetic regulations relating to somatic cell reprogramming drive tumorigenesis, highlighting the importance of epigenetic regulation in cancer development.

EXPERIMENTAL PROCEDURES

Generation of OSMK-Inducible ESCs

A 7 kb fragment containing Oct3/4-P2A-Sox2-T2A-Klf4-E2A-c-Myc-ires-mCherry cDNA was generated (Carey et al., 2009) and ligated into the pBS31 vector (Beard et al., 2006). The resulting construct was electroporated into KH2 ESCs to obtain OSKM-inducible ESCs (Beard et al., 2006). OKS-, KMS-, O-, LacZ-inducible ESCs were also generated using the KH2 ESCs system.

Mice

Chimeric mice were generated using reprogramming factor-inducible ESCs by diploid blastocyst injection. *Lgr5-EGFP-ires-CreERT2* mice were obtained from The Jackson Laboratory and were crossed with OSKM-inducible mice to obtain embryos. The compound transgenic MEFs were treated with Dox to establish the OSKM-inducible iPSCs with the *Lgr5-EGFP* reporter allele. All animal experiments were approved by the CiRA Animal Experiment Committee, and the care of the animals was in accordance with institutional guidelines.

Doxycycline Treatment

Mice at 4 or 14 weeks of age were administered 2 mg/ml Dox in their drinking water supplemented with 10 mg/ml sucrose. For cell culture, Dox was used at a concentration of 2 μg/ml.

Secondary Tumor Development

Primary kidney tumors were minced and treated with collagenase (1 U/ml) followed by 0.25% trypsin digestion. The dissociated tumor cells were inoculated subcutaneously into BALB/cSlc-*nu/nu* mice or C.B-17/Icr-*scid*Jcl mice to form transplanted secondary tumors.

RNA Preparation, qRT-PCR and Microarray Analysis

Total RNA was isolated using the RNeasy Plus Mini kit (QIAGEN). The quantitative real-time PCR analysis was performed using the GoTaq qPCR Master Mix (Promega). The specific primer pairs used for amplification are shown in Table S2. The transcript levels were normalized to the *β-actin* level. The microarray analysis was performed using the Mouse Gene 1.0 ST Array (Affymetrix) in accordance with the manufacturer's instructions. All of the data analyses were performed using the GeneSpring GX software program (version 12; Agilent Technology).

DNA Methylation Analyses

The RRBS analysis was performed as described previously (Boyle et al., 2012). The samples were sequenced on an Illumina HiSeq 2000 machine. Three-kilobase regions flanking transcription start site (from −1,500 to +1,500) were analyzed to examine DNA methylation levels. The DNA methylation levels for each gene were determined based on the median of DNA methylation values at CpG sites within the region. The DNA methylation values at CpG sites

(D) Kidney tumor-derived iPSCs can contribute to adult chimeric mice.

(E) No tumor formation was observed in the kidneys of chimeric mice generated with kidney tumor-derived iPSCs. Note that Dox treatment for 24 hr confirmed the contribution of kidney-tumor-derived iPSCs to the normal-looking kidney.

(F) The histological analyses of the kidneys of chimeric mice demonstrated no detectable histological abnormalities (a and b). Kidney-tumor-derived iPSCs labeled with Venus could contribute to normal-looking kidney (c). Scale bars, 500 μm (a) and 100 μm (b, c).

See also Figure S7.

containing higher than 10× coverage in all comparative samples were used for the analysis.

Histological Analysis and Immunostaining

Normal and tumor tissue samples were fixed in 10% buffered formalin for 24 hr and embedded in paraffin. Sections (4 μm) were stained with hematoxylin and eosin (H&E), and serial sections were used for the immunohistochemical analyses. The primary antibodies used were anti-Oct3/4 (1:100 dilution; BD Biosciences), anti-Ki-67 (1:100 dilution; Dako), anti-insulin (1:500 dilution; Dako), anti-BrdU (1:500 dilution; Abcam), anti-2A (1:250 dilution; Millipore), anti-Lin28b (1:100 dilution; Cell Signaling Technology), and anti-GFP (1:500 dilution; Invitrogen).

ACCESSION NUMBERS

The Gene Expression Omnibus accession number for the microarray and RRBS data reported in this paper is GSE52304.

SUPPLEMENTAL INFORMATION

Supplemental Information includes Extended Experimental Procedures, seven figures, and three tables and can be found with this article online at http://dx.doi.org/10.1016/j.cell.2014.01.005.

ACKNOWLEDGMENTS

We are grateful to T. Taya for CGH analysis and S. Sakurai and T. Sato for RRBS analysis. We also thank S. Masui, H. Sakurai, and members in Yamada laboratory for helpful discussions and T. Ukai, K. Osugi, and N. Nishimoto for assistance. The authors were supported in part by a Grant-in-Aid from the Ministry of Education, Culture, Sports, Science, and Technology of Japan (MEXT); the Ministry of Health, Labor, and Welfare of Japan; the JST; the Funding Program for World-Leading Innovative R&D on Science and Technology (FIRST Program) of the Japanese Society for the Promotion of Science (JSPS); the Takeda Science Foundation; and the Naito Foundation. S.Y. is a member without salary of the scientific advisory boards of iPierian, iPS Academia Japan, Megakaryon Corporation, and HEALIOS K. K. Japan. The iCeMS is supported by World Premier International Research Center Initiative, MEXT, Japan.

Received: May 29, 2013
Revised: November 6, 2013
Accepted: January 3, 2014
Published: February 13, 2014

REFERENCES

Abad, M., Mosteiro, L., Pantoja, C., Cañamero, M., Rayon, T., Ors, I., Graña, O., Megías, D., Domínguez, O., Martínez, D., et al. (2013). Reprogramming in vivo produces teratomas and iPS cells with totipotency features. Nature *502*, 340–345.

Aiden, A.P., Rivera, M.N., Rheinbay, E., Ku, M., Coffman, E.J., Truong, T.T., Vargas, S.O., Lander, E.S., Haber, D.A., and Bernstein, B.E. (2010). Wilms tumor chromatin profiles highlight stem cell properties and a renal developmental network. Cell Stem Cell *6*, 591–602.

Barker, N., van Es, J.H., Kuipers, J., Kujala, P., van den Born, M., Cozijnsen, M., Haegebarth, A., Korving, J., Begthel, H., Peters, P.J., and Clevers, H. (2007). Identification of stem cells in small intestine and colon by marker gene Lgr5. Nature *449*, 1003–1007.

Barker, N., Rookmaaker, M.B., Kujala, P., Ng, A., Leushacke, M., Snippert, H., van de Wetering, M., Tan, S., Van Es, J.H., Huch, M., et al. (2012). Lgr5(+ve) stem/progenitor cells contribute to nephron formation during kidney development. Cell Rep. *2*, 540–552.

Beard, C., Hochedlinger, K., Plath, K., Wutz, A., and Jaenisch, R. (2006). Efficient method to generate single-copy transgenic mice by site-specific integration in embryonic stem cells. Genesis *44*, 23–28.

Ben-Porath, I., Thomson, M.W., Carey, V.J., Ge, R., Bell, G.W., Regev, A., and Weinberg, R.A. (2008). An embryonic stem cell-like gene expression signature in poorly differentiated aggressive human tumors. Nat. Genet. *40*, 499–507.

Boyle, P., Clement, K., Gu, H., Smith, Z.D., Ziller, M., Fostel, J.L., Holmes, L., Meldrim, J., Kelley, F., Gnirke, A., and Meissner, A. (2012). Gel-free multiplexed reduced representation bisulfite sequencing for large-scale DNA methylation profiling. Genome Biol. *13*, R92.

Brambrink, T., Foreman, R., Welstead, G.G., Lengner, C.J., Wernig, M., Suh, H., and Jaenisch, R. (2008). Sequential expression of pluripotency markers during direct reprogramming of mouse somatic cells. Cell Stem Cell *2*, 151–159.

Carey, B.W., Markoulaki, S., Hanna, J., Saha, K., Gao, Q., Mitalipova, M., and Jaenisch, R. (2009). Reprogramming of murine and human somatic cells using a single polycistronic vector. Proc. Natl. Acad. Sci. USA *106*, 157–162.

Carey, B.W., Markoulaki, S., Beard, C., Hanna, J., and Jaenisch, R. (2010). Single-gene transgenic mouse strains for reprogramming adult somatic cells. Nat. Methods *7*, 56–59.

Ehrich, M., Nelson, M.R., Stanssens, P., Zabeau, M., Liloglou, T., Xinarianos, G., Cantor, C.R., Field, J.K., and van den Boom, D. (2005). Quantitative high-throughput analysis of DNA methylation patterns by base-specific cleavage and mass spectrometry. Proc. Natl. Acad. Sci. USA *102*, 15785–15790.

Folmes, C.D., Nelson, T.J., Martinez-Fernandez, A., Arrell, D.K., Lindor, J.Z., Dzeja, P.P., Ikeda, Y., Perez-Terzic, C., and Terzic, A. (2011). Somatic oxidative bioenergetics transitions into pluripotency-dependent glycolysis to facilitate nuclear reprogramming. Cell Metab. *14*, 264–271.

Fussner, E., Djuric, U., Strauss, M., Hotta, A., Perez-Iratxeta, C., Lanner, F., Dilworth, F.J., Ellis, J., and Bazett-Jones, D.P. (2011). Constitutive heterochromatin reorganization during somatic cell reprogramming. EMBO J. *30*, 1778–1789.

Hochedlinger, K., Yamada, Y., Beard, C., and Jaenisch, R. (2005). Ectopic expression of Oct-4 blocks progenitor-cell differentiation and causes dysplasia in epithelial tissues. Cell *121*, 465–477.

Hong, H., Takahashi, K., Ichisaka, T., Aoi, T., Kanagawa, O., Nakagawa, M., Okita, K., and Yamanaka, S. (2009). Suppression of induced pluripotent stem cell generation by the p53-p21 pathway. Nature *460*, 1132–1135.

Jones, P.A., and Baylin, S.B. (2002). The fundamental role of epigenetic events in cancer. Nat. Rev. Genet. *3*, 415–428.

Kim, J., Woo, A.J., Chu, J., Snow, J.W., Fujiwara, Y., Kim, C.G., Cantor, A.B., and Orkin, S.H. (2010). A Myc network accounts for similarities between embryonic stem and cancer cell transcription programs. Cell *143*, 313–324.

Kobayashi, A., Valerius, M.T., Mugford, J.W., Carroll, T.J., Self, M., Oliver, G., and McMahon, A.P. (2008). Six2 defines and regulates a multipotent self-renewing nephron progenitor population throughout mammalian kidney development. Cell Stem Cell *3*, 169–181.

Maherali, N., Sridharan, R., Xie, W., Utikal, J., Eminli, S., Arnold, K., Stadtfeld, M., Yachechko, R., Tchieu, J., Jaenisch, R., et al. (2007). Directly reprogrammed fibroblasts show global epigenetic remodeling and widespread tissue contribution. Cell Stem Cell *1*, 55–70.

Meissner, A., Gnirke, A., Bell, G.W., Ramsahoye, B., Lander, E.S., and Jaenisch, R. (2005). Reduced representation bisulfite sequencing for comparative high-resolution DNA methylation analysis. Nucleic Acids Res. *33*, 5868–5877.

Mikkelsen, T.S., Ku, M., Jaffe, D.B., Issac, B., Lieberman, E., Giannoukos, G., Alvarez, P., Brockman, W., Kim, T.K., Koche, R.P., et al. (2007). Genome-wide maps of chromatin state in pluripotent and lineage-committed cells. Nature *448*, 553–560.

Mikkelsen, T.S., Hanna, J., Zhang, X., Ku, M., Wernig, M., Schorderet, P., Bernstein, B.E., Jaenisch, R., Lander, E.S., and Meissner, A. (2008). Dissecting direct reprogramming through integrative genomic analysis. Nature *454*, 49–55.

Ogawa, O., Eccles, M.R., Szeto, J., McNoe, L.A., Yun, K., Maw, M.A., Smith, P.J., and Reeve, A.E. (1993). Relaxation of insulin-like growth factor II gene imprinting implicated in Wilms' tumour. Nature *362*, 749–751.